

## Durham Research Online

---

### Deposited in DRO:

17 November 2015

### Version of attached file:

Accepted Version

### Peer-review status of attached file:

Peer-reviewed

### Citation for published item:

Ullah, Z. and Coombs, W. M. and Augarde, C. E. (2016) 'Parallel computations in nonlinear solid mechanics using adaptive finite element and meshless methods.', *Engineering computations.*, 33 (4). pp. 1161-1191.

### Further information on publisher's website:

<http://dx.doi.org/10.1108/ec-06-2015-0166>

### Publisher's copyright statement:

This article is © Emerald Group Publishing and permission has been granted for this version to appear here <http://dro.dur.ac.uk/16820/>. Emerald does not grant permission for this article to be further copied/distributed or hosted elsewhere without the express permission from Emerald Group Publishing Limited.

### Additional information:

## Use policy

---

The full-text may be used and/or reproduced, and given to third parties in any format or medium, without prior permission or charge, for personal research or study, educational, or not-for-profit purposes provided that:

- a full bibliographic reference is made to the original source
- a [link](#) is made to the metadata record in DRO
- the full-text is not changed in any way

The full-text must not be sold in any format or medium without the formal permission of the copyright holders.

Please consult the [full DRO policy](#) for further details.

# Parallel computations in nonlinear solid mechanics using adaptive finite element and meshless methods

Z. Ullah<sup>a1</sup>, W. M. Coombs<sup>b</sup>, C. E. Augarde<sup>b</sup>

<sup>a</sup>School of Engineering, Rankine Building, The University of Glasgow, Glasgow, G12 8LT, UK

<sup>b</sup>School of Engineering and Computing Sciences, Durham University, Durham, DH1 3LE, UK

## Structured abstract

### Purpose

A variety of meshless methods have been developed in the last twenty years with an intention to solve practical engineering problems, but are limited to small academic problems due to associated high computational cost as compared to the standard finite element methods (FEM). The main purpose of this paper is the development of an efficient and accurate algorithms based on meshless methods for the solution of problems involving both material and geometrical nonlinearities.

### Design/methodology/approach

A parallel two-dimensional linear elastic computer code is presented for a maximum entropy basis functions based meshless method. The two-dimensional algorithm is subsequently extended to three-dimensional adaptive nonlinear and three-dimensional parallel nonlinear adaptively coupled finite element, meshless method cases. The Prandtl-Reuss constitutive model is used to model elasto-plasticity and total Lagrangian formulations are used to model finite deformation. Furthermore, Zienkiewicz & Zhu and Chung & Belytschko error estimation procedure are used in the FE and meshless regions of the problem domain respectively. The MPI library and open-source software packages, METIS and MUMPS are used for the high performance computation.

### Findings

Numerical examples are given to demonstrate the correct implementation and performance of the parallel algorithms. The agreement between the numerical and analytical results in the case of linear-elastic example is excellent. For the non-linear problems load displacement curve are compared with the reference FEM and found in a very good agreement. As compared to the FEM, no volumetric locking was observed in the case of meshless method. Furthermore, it is shown that increasing the number of processors up to a given number improve the performance

<sup>1</sup>Correspondence to: Z. Ullah, E-mail: Zahur.Ullah@glasgow.ac.uk

of parallel algorithms in term of simulation time, speedup and efficiency.

### Originality/value

Problems involving both material and geometrical nonlinearities are of practical importance in many engineering applications, e.g. geomechanics, metal forming and biomechanics. A family of parallel algorithms has been developed in this paper for these problems using adaptively coupled finite-element, meshless method (based on maximum entropy basis functions) for distributed memory computer architectures.

## 1 Introduction

In almost every scientific field including academia and industry, complexity and size of problems increases with time. For solution of these problems, computers with very large memory and very high computational power are required. Conventional sequential computers cannot handle these large and complicated problems due to their limited memory and computational power. Parallel computations have been used to solve these problems very conveniently, working on the “divide-and-conquer” strategy (Pacheco, 1997). Using this strategy a very large and computationally demanding problem is divided into small manageable subproblems and each is then assigned to a different computer. Parallel computations are now commonly used in almost every scientific field. Different types of parallel computers are now widely available, mostly based on either shared memory or distributed memory computer architectures.

The finite element method (FEM) is the most prominent used numerical technique for the solution of practical problems in different scientific fields. In the FEM, the memory requirement and corresponding computational demand increases with the number of degrees of freedom, therefore, parallel computations have been used extensively in the FEM, the details of which can be found in many references, including (Grosso and Righetti, 1988; Becene, 2003; Yagawa et al., 1991; Luo and Friedman, 1990; Chiang and Fulton, 1990; Carter et al., 1989). The domain decomposition method is the traditional way to divide a large FEM problem into smaller subproblems, in which load balancing and inter-processor communication are two important parameters. For good performance of parallel programs, equal computational load must be assigned to each processor to minimise the waiting, or idle, whilst minimising inter-processor communication. Different strategies have been used in the literature for domain decomposition, including graph-based techniques (Karypis and Kumar, 1998; Walshaw et al., 1995; Leland and Hendrickson, 1995) and geometry-based techniques (Jones and Plassmann, 1994; Danielson et al., 2000). Graph based techniques are normally used in the FEM due to reasons of accuracy

and efficiency.

As compared to the FEM, meshless methods are ideal for modelling certain types of problems, e.g. problems with large deformation, material damage, projectile penetration, fragmentation, crack growth and moving boundaries (Zhuang et al., 2012a), their computational inefficiency restricts their use in practice to date to simple academic problems. Here one of the most commonly used meshless methods, the element-free Galerkin method (EFGM) (Belytschko et al., 1994), is adopted. However, maximum entropy basis functions (max-ent) (Sukumar, 2004; Arroyo and Ortiz, 2006; Sukumar and Wright, 2007) are used instead of the standard moving least squares basis functions. This provides direct imposition of the essential boundary conditions and also provides a natural way to couple the meshless methods with the FE regions as compared to the use of moving least squares basis functions, which need extra care to properly couple the same regions. Furthermore, as compared to the corresponding MLS counterparts, construction of basis functions and corresponding basis function derivatives are more efficient in the case of max-ent. Recent use of the max-ent method, e.g. in fracture mechanics, can be found in Amiri et al. (2014b,a), while other recent examples of the use of max-ent in meshless methods can be found in (Ortiz et al., 2010, 2011; Millán et al., 2011; Quaranta et al., 2012; Rosolen et al., 2012; Millán et al., 2015; Peco et al., 2015).

Meshless methods are superior to the finite element method (FEM) in terms of accuracy and convergence but are computationally more expensive. Therefore, it is more practical to use a meshless method only in regions of a problem domain requiring its high accuracy, where it can outperform the FEM, while using the FEM in the remaining part of the problem domain. For this combined method, proper coupling between the FEM and the meshless method is essential for accurate results. Previous research has used interface elements between EFG and FE regions (Belytschko et al., 1995). This approach was motivated by the incompatibility between the MLS basis functions within the EFG region for the approximation of the field variables, and the standard polynomial shape functions in the FE region. The FE-EFGM coupling procedure of Belytschko et al. (1995) has since been extended for the case of EFG nodal integration by Belytschko et al. (1998). A continuous blending method for the FE-EFGM coupling was introduced by Fernández-Méndez and Huerta (2000) and Huerta et al. (2004) with some advantages compared to the FE-EFGM coupling procedure of Belytschko et al. (1995) since ramp functions and the use of the FE nodes as the EFG nodes are not required, therefore, EFG nodes can also be added within the transition region. Lagrange multipliers were used for linear elastic analysis with the same type of coupling in Hegen (1996), an idea that was later extended to nonlinear reinforced concrete problems in Rabczuk and Belytschko (2006), where reinforcement was modelled with the FEM and concrete with the EFGM. In Gu and Zhang (2008), a transition (or bridging region) was used for coupling between the FEM and a

meshless method. The transition region was discretized by particles, which were independent of both the FE and meshless nodes. A detailed review of this type of coupling between the EFGM and the FEM can be found in [Rabczuk et al. \(2006\)](#). A coupled FE-EFGM was also proposed in [Wang et al. \(2009\)](#) for the simulation of automotive crash tests, in which areas of very high deformation were modelled with the EFGM. This work used constraints to ensure the continuity of the field variables across the FE-EFGM interface without using interface elements. A slight variation of the FE-EFGM coupling with interface elements ([Belytschko et al., 1995](#)), in which there was no need for a pre-existing transition region between the FE and EFG regions, was proposed in [Rao and Rahman \(2001\)](#). The method was applied to the simulation of linear elastic fracture mechanics problems, including mode-I, mode-II and mixed mode problems. The area near the crack was modelled with the EFGM, while the FEM was used in the remaining part of the problem domain. A coupled FE-EFGM procedure based on a collocation approach was proposed by [Xiao and Dhanasekar \(2002\)](#), in which at the interface between the FE and the EFG regions, fictitious nodal values were converted to real nodal displacements using the MLS basis functions and were assigned back to the FE nodes. Meshless methods have also been with other numerical methods, e.g. isogeometric analysis (IGA), in which IGA was used on the problem boundaries for exact geometry representation. In [Wang and Zhang \(2014\)](#) and [Valizadeh et al. \(2015\)](#) RKPM was coupled with IGA and the method was used for two- and three-dimensional linear-elastic problems, while in [Rosolen and Arroyo \(2013\)](#) max-ent was coupled with IGA and was applied to two-dimensional heat conduction, linear and non-linear elasticity examples. Other related numerical method for fracture modelling are extended isogeometric element formulation (XIGA) ([Nguyen-Thanh et al., 2015](#)) and a continuous/discontinuous deformation analysis (CDDA) method ([Cai et al., 2013](#)).

In this paper, a parallel algorithm is presented based on distributed memory computer architecture for linear and adaptive nonlinear meshless method (based on maximum entropy basis functions), which is then extended to nonlinear adaptively coupled FE-meshless method. The details of the sequential version of these methods can be found in our recent publications [Ullah and Augarde \(2013\)](#) and [Ullah et al. \(2013a,c\)](#) respectively. A total Lagrangian formulation is used to model finite deformation and the Prandtl-Reuss constitutive model is used to model elasto-plasticity. Codes were developed based on these algorithms in FORTRAN 90 with other supporting libraries, including NAG, Voro++ ([Rycroft, 2007](#); [Rycroft et al., 2006](#)) and kd-tree ([Cormen et al., 2009](#); [Moore, 1991](#); [Kennel, 2004](#); [Barbieri and Meo, 2012](#); [Ullah, 2013](#)). NAG library is used for simple linear algebra, including multiplication of small matrices, matrix inversion and calculation of eigen values and eigen vectors. For three-dimensional problems with unstructured nodes, results from an adaptive analysis, calculation of the proper nodal domains of influence is very challenging. For these problems, three-dimensional Voronoi diagrams are

very useful to calculate the influence domains, for which Voro++ library is used here, further detail of this procedure is given in [Ullah \(2013\)](#). Voro++ is an open-source software library for the calculation of three-dimensional Voronoi diagrams for a set of particles in space, written in C++. The Message passing interface(MPI) library was used for inter-processor communication, further details of which can be found in more specialised references, such as ([Slim, 2010](#); [Gropp et al., 1999a,b,a](#); [Snir et al., 1998](#); [Gropp et al., 1998](#); [Pacheco, 2011](#); [Rauber and Rünger, 2010](#)). Furthermore, the open-source software packages, METIS ([Karypis, 2011](#)) and Multifrontal Massively Parallel Solver (MUMPS) ([MUMPS, 2011](#)) were used to automatically divide the problem domain and for the solution of the final system of linear equations in parallel, respectively. The codes have been run successfully on the Durham University high performance cluster, Hamilton. Performance parameters used for the parallel programs are simulation time, speedup and efficiency.

Parallel computing has been attempted in a number of references for the EFGM. In [Vacharasintopchai \(2000\)](#), parallel three-dimensional EFGM code was developed for linear-elastic problems. In this study Parallel computer was constructed by joining several low cost computers with a high-speed network and the MPI library was used for the inter-processor communication. Accuracy, run time, speedup and efficiency were used to measure the performance of the parallel program for benchmark numerical problems. Several numerical examples were solved and good accuracy was obtained for stresses and displacements relative to the analytical and sequential counterpart solutions. However, the approach was limited to linear elastic problems and was shown to give promising results for problems up to only 1000 degrees of freedoms. In [Singh and Jain \(2005\)](#), EFGM code is described using a sparse linear solver based on data decomposition strategy. The code was validated on three-dimensional heat transfer problems with the same performance parameters. The dual finite element tearing and interconnecting (FETI) ([Farhat and Roux, 1991](#)), was used for the EFGM in [Metsis and Papadrakakis \(2012\)](#). In [Rabczuk and Belytschko \(2005\)](#) h-adaptivity is implemented for linear and non-linear dynamics problems for a structured particle coinciding with background integration mesh, which leads to simple data structures. The method proposed in [Rabczuk and Belytschko \(2005\)](#) is later used in [Rabczuk and Belytschko \(2007\)](#) for arbitrary oriented cracks in three-dimensions and in [Rabczuk and Samaniego \(2008\)](#) for modelling shear band with cohesive surfaces.

In the reproducing kernel particle method (RKPM) ([Liu et al., 1995](#)), parallel computation has also been used in a number of references. In [Wang et al. \(2007\)](#), a parallel code was developed for the RKPM to simulate three-dimensional bulk metal forming. Integration cells were divided among the processors using the domain decomposition method and nodes/particles were then duplicated accordingly. As compared to the FEM, the high communication cost in the case of meshless methods was also mentioned in this study. A von-Mises constitutive model with

linear isotropic hardening was used to model elasto-plasticity. Taylor bar impact and backward extrusion were used as test problems to show the performance of the parallel algorithm and results were compared with the reference FEM approach using 8-node hex elements. For explicit dynamics analysis, a parallel code based on the MPI library was developed in [Danielson et al. \(2000\)](#). Integration points were used for partitioning instead of the background cells because of the different number of nodes in the support of each Gauss point, which leads to different computational loads associated with each Gauss point. Nodes/particles were then duplicated accordingly. It was shown that the METIS partitions were almost perfectly balanced. It was also mentioned that the communication cost in the case of the parallel RKPM algorithm is larger than the corresponding parallel FEM algorithm. Three-point bending of a notched beam and three-dimensional shear band simulation in a tensile specimen were used as numerical examples to show the performance of this parallel code. In [Günther et al. \(2000\)](#), a parallel RKPM code based on the distributed memory computer architecture was developed to solve viscous compressible flow problems. In [Rabczuk and Eibl \(2003\)](#), concrete fragmentation under explosive loading is modelled by SPH and is implemented in FORTRAN 90 with MPI library. Parallel computing has also been used for other meshless methods for example see [Shirazaki and Yagawa \(1999\)](#), [Medina and Chen \(2000\)](#) and [Hu et al. \(2007\)](#). In the current paper, a family of parallel computer algorithms is developed based on distributed memory computer architecture for two-dimensional linear elastic meshless method, three-dimensional adaptive nonlinear meshless method and three-dimensional nonlinear adaptively coupled finite element-meshless method. The meshless method algorithms including error estimation, adaptivity, adaptive FE-meshless method coupling were already covered in our previous publications ([Ullah and Augarde, 2010](#); [Ullah et al., 2011, 2012, 2013b](#); [Ullah and Augarde, 2013](#); [Ullah et al., 2013a,c](#); [Ullah, 2013](#)), but for completeness aspects, the main components pertinent to the parallel implementation are repeated here.

This paper is organised as follows. A short summary of the basic equations of the max-ent basis functions based meshless method is given in §2. Comparison of the computational cost for the construction of MLS and max-ent basis functions and corresponding derivatives are given §3. Performance indicators of the parallel computer program, including speedup and efficiency are introduced in §4. The parallel linear elastic meshless method algorithm and its implementation are described in §5. The parallel linear elastic meshless method algorithm is extended to parallel adaptive nonlinear meshless method case in §6, which is further extended to parallel nonlinear adaptively coupled FE-meshless method in §7. Finally, the three developed parallel algorithms are validated with numerical examples in §8. Concluding remarks to this paper are given in §9.



## 2 Max-ent basis function based meshless method

For completeness of the paper, a short summary of the basic equations of the max-ent basis functions based meshless method is provided here, details of which can be found in Ullah (2013) and Ullah et al. (2013c). A three-dimensional formulations is given, but it is straightforward to modify this for one- and two-dimensional cases. The final discrete system of linear equations is written as

$$\mathbf{K}\mathbf{u} = \mathbf{f}, \quad (1)$$

where

$$\mathbf{K}_{ij} = \int_{\Omega} \mathbf{B}_i^T \mathbf{D} \mathbf{B}_j d\Omega, \quad (2)$$

$$\mathbf{f}_i = \int_{\Gamma_t} \phi_i \bar{\mathbf{t}} d\Gamma + \int_{\Omega} \phi_i \mathbf{b}_f d\Omega, \quad (3)$$

$$\mathbf{B}_i = \begin{bmatrix} \frac{\partial \phi_i}{\partial x} & 0 & 0 \\ 0 & \frac{\partial \phi_i}{\partial y} & 0 \\ 0 & 0 & \frac{\partial \phi_i}{\partial z} \\ \frac{\partial \phi_i}{\partial y} & \frac{\partial \phi_i}{\partial x} & 0 \\ \frac{\partial \phi_i}{\partial z} & 0 & \frac{\partial \phi_i}{\partial x} \\ 0 & \frac{\partial \phi_i}{\partial z} & \frac{\partial \phi_i}{\partial y} \end{bmatrix}, \quad (4)$$



and

$$\mathbf{D} = \frac{E}{(1+\nu)(1-2\nu)} \begin{bmatrix} 1-\nu & \nu & \nu & 0 & 0 & 0 \\ \nu & 1-\nu & \nu & 0 & 0 & 0 \\ \nu & \nu & 1-\nu & 0 & 0 & 0 \\ 0 & 0 & 0 & \frac{1-2\nu}{2} & 0 & 0 \\ 0 & 0 & 0 & 0 & \frac{1-2\nu}{2} & 0 \\ 0 & 0 & 0 & 0 & 0 & \frac{1-2\nu}{2} \end{bmatrix}. \quad (5)$$

Where  $\nu$  is the Poisson's ratio and  $E$  is the modulus of elasticity. To perform the integrations in (2) and (3) numerically, the problem domain  $\Omega$  and traction boundary  $\Gamma_t$  are divided into a number of non-overlapping background cells. In Equation (1)  $\mathbf{u}$  are known as fictitious nodal values or nodal parameters and  $\phi_i$  is a matrix of the max-ent basis functions for node  $i$  at a point  $\mathbf{x}$ , where

$$\phi_i = \begin{bmatrix} \phi_i & 0 & 0 \\ 0 & \phi_i & 0 \\ 0 & 0 & \phi_i \end{bmatrix}. \quad (6)$$

The max-ent shape functions can be defined as

$$\phi_i = \frac{Z_i}{Z} \quad (7)$$

where

$$Z_i = w_i e^{-\lambda_1 \tilde{x}_i - \lambda_2 \tilde{y}_i - \lambda_3 \tilde{z}_i} \quad \text{and} \quad Z = \sum_{j=1}^n Z_j, \quad (8)$$

in which  $w_i$  is the weight function associated with node  $i$ , evaluated at point  $\mathbf{x} = (x, y)^T$ ,  $\tilde{x}_i = x_i - x$ ,  $\tilde{y}_i = y_i - y$  and  $\tilde{z}_i = z_i - z$  are shifted coordinates.  $n$  is the number of nodes in support of Gauss point  $\mathbf{x}$  (nodes, the influence domains of whose encompass the Gauss point) and  $\lambda_1$ ,  $\lambda_2$  and  $\lambda_3$  are Lagrange multipliers which can be found from

$$(\lambda_1, \lambda_2, \lambda_3) = \operatorname{argmin} F(\lambda_1, \lambda_2, \lambda_3) \quad \text{where} \quad F(\lambda_1, \lambda_2, \lambda_3) = \log(Z). \quad (9)$$

$F$  is a convex function and Newton's method is used to solve (9) to find the Lagrange multipliers which can then be used in the expressions for the shape functions (Sukumar, 2004; Arroyo and

Ortiz, 2006; Sukumar and Wright, 2007). The shape function derivatives follow as

$$\nabla \phi_i = \phi_i \left( \nabla f_i - \sum_{i=1}^n \phi_i \nabla f_i \right), \quad (10)$$

where

$$\nabla f_i = \frac{\nabla w_i}{w_i} + \boldsymbol{\lambda} + \tilde{\mathbf{x}}_i [\mathbf{H}^{-1} - \mathbf{H}^{-1} \mathbf{A}] \quad \text{and} \quad \mathbf{A} = \sum_{k=1}^n \phi_k \tilde{\mathbf{x}}_k \otimes \frac{\nabla w_k}{w_k}. \quad (11)$$

Where  $\mathbf{H}$  is the Hessian matrix and the dyadic product  $\otimes$  of two vector  $\mathbf{a}$  and  $\mathbf{b}$  is a second order tensor, i.e.  $\mathbf{a} \otimes \mathbf{b}$  defined as  $\mathbf{a} \otimes \mathbf{b} = \mathbf{a} \mathbf{b}^T$ . In the case of nonlinear problems, a total Lagrangian formulation is used to model finite deformation and for modelling elasto-plasticity, the Prandtl-Reuss constitutive model is used, details of which can be found in Ullah et al. (2013c).

### 3 Computational cost of max-ent versus MLS basis functions

To compare the computational cost for construction of MLS and max-ent basis functions and corresponding basis function derivatives, a cube is considered with 10 unit dimensions in the  $x$ ,  $y$  and  $z$  directions. Seven different discretisations are considered in this case with 125, 343, 729, 1331, 2197, 3375 and 4913 uniformly distributed nodes in the consecutive discretizations, while the number of background cells used in the consecutive discretisations are 64, 216, 512, 1000, 1728, 2744 and 4096. Three sample discretizations with 125, 729 and 2197 nodes are shown in Figures 1(a-c) respectively. Furthermore,  $64 (4 \times 4 \times 4)$  Gauss points are used in each background cell and the scaling parameter used for the domain of influence is  $d_{max} = 1.5$ . For the calculation of MLS basis functions, linear polynomial basis functions are considered while the max-net basis functions are calculated using the Newton-Raphson method with a convergence criterion of  $10^{-6}$  (Ullah, 2013). The computational cost for the construction of MLS and max-ent basis functions and corresponding derivatives for all the Gauss points are shown in Table 1, which clearly demonstrate the computational efficiency of max-ent basis functions and corresponding derivatives over MLS counterpart for given polynomial basis function in MLS and convergence criterion of Newton's method for the max-ent.

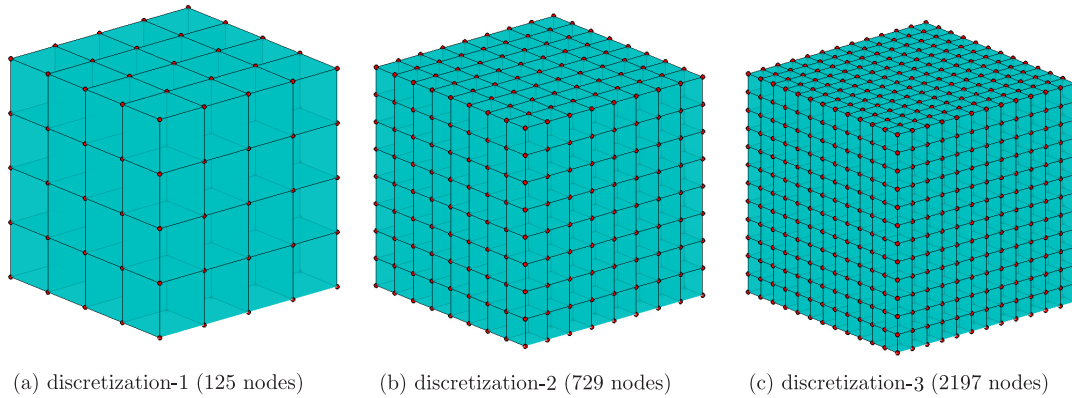


Figure 1: Sample discretizations used for the run time comparison of max-ent and MLS basis functions

Nodes	Background Cells	Number of Gauss points	max-ent (sec)	MLS (sec)
125	64	4096	0.83	0.83
343	216	13824	3.15	3.34
729	512	32768	8.21	8.71
1331	1000	64000	14.5	16.84
2197	1728	110592	26.15	28.02
3375	2744	175616	47.06	53.49
4913	4096	262144	72.25	78.18

Table 1: Comparison of computational cost of max-ent and MLS basis functions

## 4 Performance indicators for parallel programs

Computational efficiency is one of the main purposes of writing a parallel program. Therefore, run time of a parallel program must be compared with the corresponding run time of a sequential equivalent. Speedup and efficiency are the two measures that are commonly used to evaluate the performance of a parallel program, the detail of which can be found in Pacheco (2011), Rauber and Rünger (2010) and Slim (2010); Gropp et al. (1999a). Run/simulation time and cost of parallel computation are also important parameters required for understanding speedup and efficiency. For a sequential program, **run time** is the time between the start and end of simulation, while for a parallel program, it is the time between the start of simulation and end of computation on the last processor. The **cost** of a parallel computation  $C_n$  is the time taken by all processors involved in the computation, i.e.

$$C_n = nT_n, \quad (12)$$

where  $n$  is the number of processors and  $T_n$  is the time the program spends on  $n$  processors (parallel run time) (Rauber and Rünger, 2010). **Speedup**  $S_n$  is the ratio of the time a parallel program spends on one processor  $T_1$  to the time the same program spends on  $n$  processors  $T_n$ , that is

$$S_n = \frac{T_1}{T_n}. \quad (13)$$

In an ideal situation  $S_n = n$  but generally  $S_n \leq n$  due to additional work done by a parallel program, known as overhead. This overhead consists of communication between the processors, synchronization, idle time for some processors due to unbalanced load and redundant calculation to avoid data transfer. Furthermore, it is impossible to 100% parallelize a code due to its sequential parts, especially input and output. **Efficiency**  $E_n$  is the ratio of the total simulation time by all the processors to the simulation time by a single processor, or alternatively it is defined as the ratio of the number of processors to speedup, i.e.

$$E_n = \frac{nT_n}{T_1} = \frac{n}{S_n}. \quad (14)$$

In an ideal situation  $E_n = 1$  but generally  $E_n \leq 1$ .

## 5 Parallel linear elastic algorithm

The parallel algorithm for the meshless method for linear elastic problems is described here, and is extended to the adaptive nonlinear and nonlinear adaptively coupled FE-meshless method cases in the following sections. Before explaining the parallel meshless method algorithm, a comparison is given of the computation involved in the parallel meshless method and the parallel FEM algorithm. Sample partitions for two processors for the FEM and the meshless method are shown in Figures 2(a) and 2(b) respectively. In the FEM case, the boundary nodes between the two processors are required on both processors for the calculation of the basis functions and corresponding basis function derivatives. These nodes are shown as solid black circles in Figure 2(a) and should be duplicated on both processors. These shared nodes represent the communication cost, i.e. the information required to be transferred between the two processors. As compared to the FEM, in the meshless method case, more nodes are required for the calculation of basis functions and corresponding basis function derivatives as shown in Figure 2(b), therefore more nodes need to be shared between the processors in the meshless method case. As Figure 2(b) shows, the influence domains of nodes shown in red covers Gauss points that belong to the other processor, therefore, these nodes must be duplicated. This

increase in the shared nodes as compared to the FEM case, increases the communication cost in the meshless method case.

The flow chart for the parallel algorithm for the meshless method for linear elastic problems is shown in Figure 3, all of which have been implemented from scratch by the first author in FORTRAN with NAG, MPI, METIS, MUMPS, KDTree and Voro++ supporting libraries. The two computationally expensive parts, i.e. assembly of the stiffness matrix and the solution of the final system of linear equations, are performed in parallel. At the start of the analysis, the MPI library is initialized and the problem is set up on each processor involved in the computation, to reduce the inter-processor communication. The problem setup includes the definition of nodal coordinates, background cells, Gauss points and influence domains. Input data is then prepared for METIS for domain decomposition, the detail of which can be found in Karypis (2011). METIS library subroutine "METIS.PartMeshDual" is used here for this purpose, which directly divides the background integration cells into the user defined number of subdomains. The output of "METIS.PartMeshDual" is "epart" is a vector of length equal to the number of background cells where each entry shows the processor number to which the background cell belongs. For each Gauss point, the Kd-tree with background mesh algorithm (Barbieri and Meo, 2012; Ullah, 2013) is used to search nodes whose influence domains encompass the Gauss point (here referred to as nodes in the support of Gauss point). The subsequent step is the assembly of stiffness matrices on each processor using the MUMPS distributed assembled matrix format. The size of the stiffness matrix on each processor depends on the nodes, which are in support of its Gauss points, see Figure 2(b). Shared nodes must be included in the list of nodes for both processors. The stiffness matrix on each processor is then calculated and assembled. Force vector  $\mathbf{f}$  is assembled only on the host or master processor. Input data are then prepared for MUMPS for the solution of the final system of linear equations, the detail of which can be found in MUMPS (2011). Finally, output data, e.g. displacements and stresses, are calculated before finalizing the MPI library and ending the analysis.

## 6 Parallel adaptive nonlinear algorithm

In this section, the parallel algorithm described previously for the meshless method for linear elastic problems is extended to three-dimensional adaptive problems with both material and geometrical nonlinearities. A total Lagrangian formulation is used here to model finite deformation and the Prandtl-Reuss constitutive model is used to model elasto-plasticity. The algorithm given here is based on the sequential two-dimensional adaptively nonlinear meshless method given in our previous publications Ullah and Augarde (2013) and Ullah (2013) where

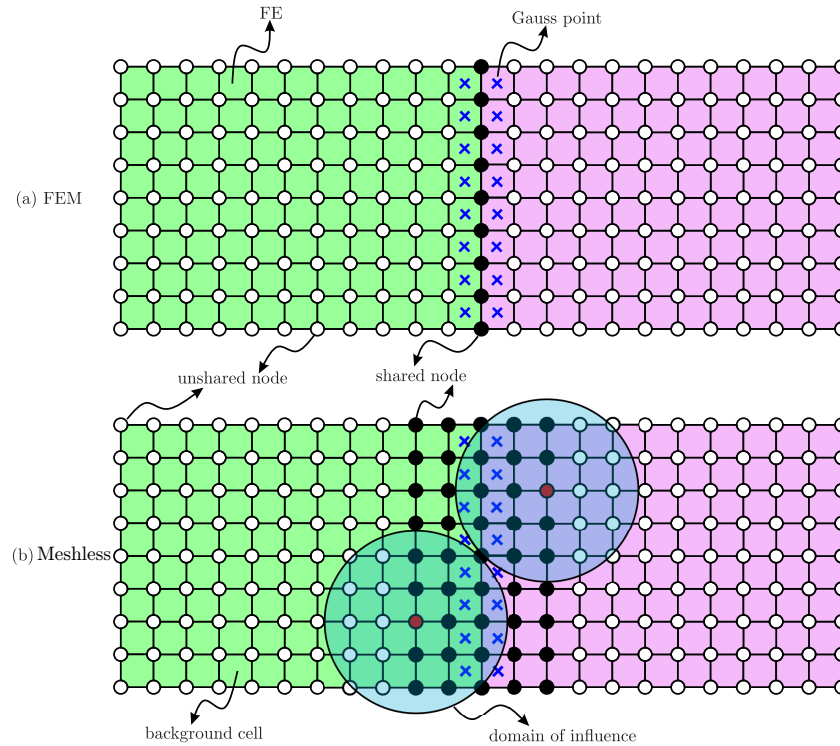


Figure 2: Sample partitions on two processors for (a) FEM and (b) Meshless method

the mathematical background can be found, which is not repeated here for the sake of brevity. The flow chart of the parallel algorithm in this case is shown in Figure 4. A total Lagrangian formulation is used here to model finite deformation and the Prandtl-Reuss constitutive model is used to model elasto-plasticity. Here the start of the algorithm is almost the same as given for the linear elastic case, i.e. the definition of the problem and METIS partitioning. Nodal influence domains for analysis (used to calculate the basis functions and derivatives used to assemble the stiffness matrices) and projection (used to calculate the strains and stresses for the error estimation based on the procedure given in Chung and Belytschko (1998) and Ullah and Augarde (2013)) are calculated on the host and are broadcast to all other processors involved in the computation. Kd-tree with background mesh algorithm is then used to calculate nodes in support of each Gauss point, for both analysis and projection. The Kd-tree is also used to find nodes in support at each node location for the calculation of nodal strains and stresses used in the calculation of the error estimates. For each processor, basis functions and corresponding basis function derivatives are calculated for analysis at each Gauss point belonging to it and are stored in separate files. The same procedure is repeated for the calculation of basis functions at each Gauss point for projection, and the calculation of basis functions and corresponding basis function derivatives at each node for the calculation of nodal strains and stresses. Determination of the size of the stiffness matrix on each processor and calculation

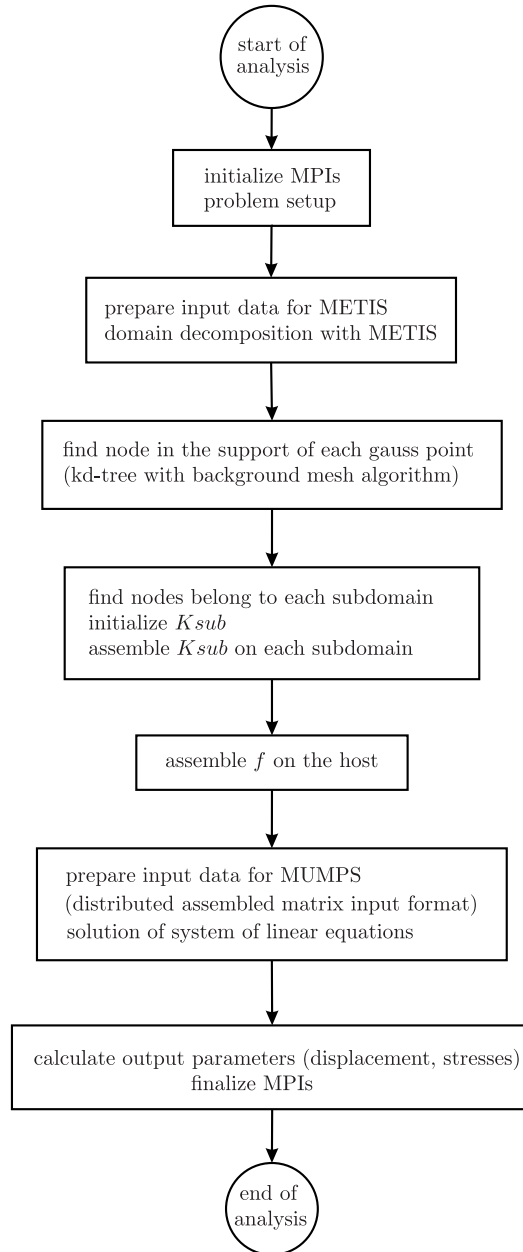


Figure 3: Linear elastic parallel algorithm



and assembly of the stiffness matrix is then performed in parallel in the same way as explained previously for the linear elastic case.

For load step  $n$ , systems of linear equations are solved in parallel with MUMPS, using the distributed assembled matrix input format. Internal and reaction forces are calculated next in parallel separately on each processor and are combined on the host to calculate the out-of-balance force, which is then used to control the Newton-Raphson iteration procedure. After convergence of the Newton-Raphson iterations, the next step is the calculation of nodal strains and stresses for error estimation. METIS also gives nodal partitions, which are used here to calculate the nodal strains and stresses in parallel. The error is also estimated in parallel here because the Chung & Belytschko error estimation procedure works cell-wise. Therefore, error is calculated separately on each processor and then combined to calculate the global error. The global error is then used to control the adaptive process, as already explained in [Ullah and Augarde \(2013\)](#). Transfer of the path dependent variables both for the nodes and the Gauss points is performed in parallel. After each refinement, METIS is used for automatic domain decomposition.

## 7 Parallel nonlinear adaptively coupled FE-meshless method algorithm

The final step is to extend the method described in the previous section to include adaptive FE-meshless method coupling. The details of the sequential version are given in [Ullah et al. \(2013c\)](#) and are not repeated here. In this new algorithm, a coupled FE-meshless method discretisation consisting of both FEs and meshless method background cells is partitioned with METIS, where each METIS partition can consist of both FEs and meshless method background cells. Kd-tree with background mesh algorithm is then used to find nodes in the support of those Gauss points, which belong to the meshless method region of the problem domain. The error for the coupled FE-meshless method discretisation, is calculated using both the Zienkiewicz & Zhu ([Zienkiewicz and Zhu, 1992a,b](#); [Boroomand and Zienkiewicz, 1999](#)) and the Chung & Belytschko error estimators for the FE and meshless method regions of the problem domain respectively. The combined procedure using both the Zienkiewicz & Zhu and the Chung & Belytschko error estimation procedure for the coupled FE-meshless method discretisation is given in detail in our previous publication ([Ullah et al., 2013c](#)) and is not repeated here. Nodal incremental strains and stresses are calculated sequentially in contrast to the previous parallel nonlinear adaptive meshless method algorithm. The superconvergent patch recovery method

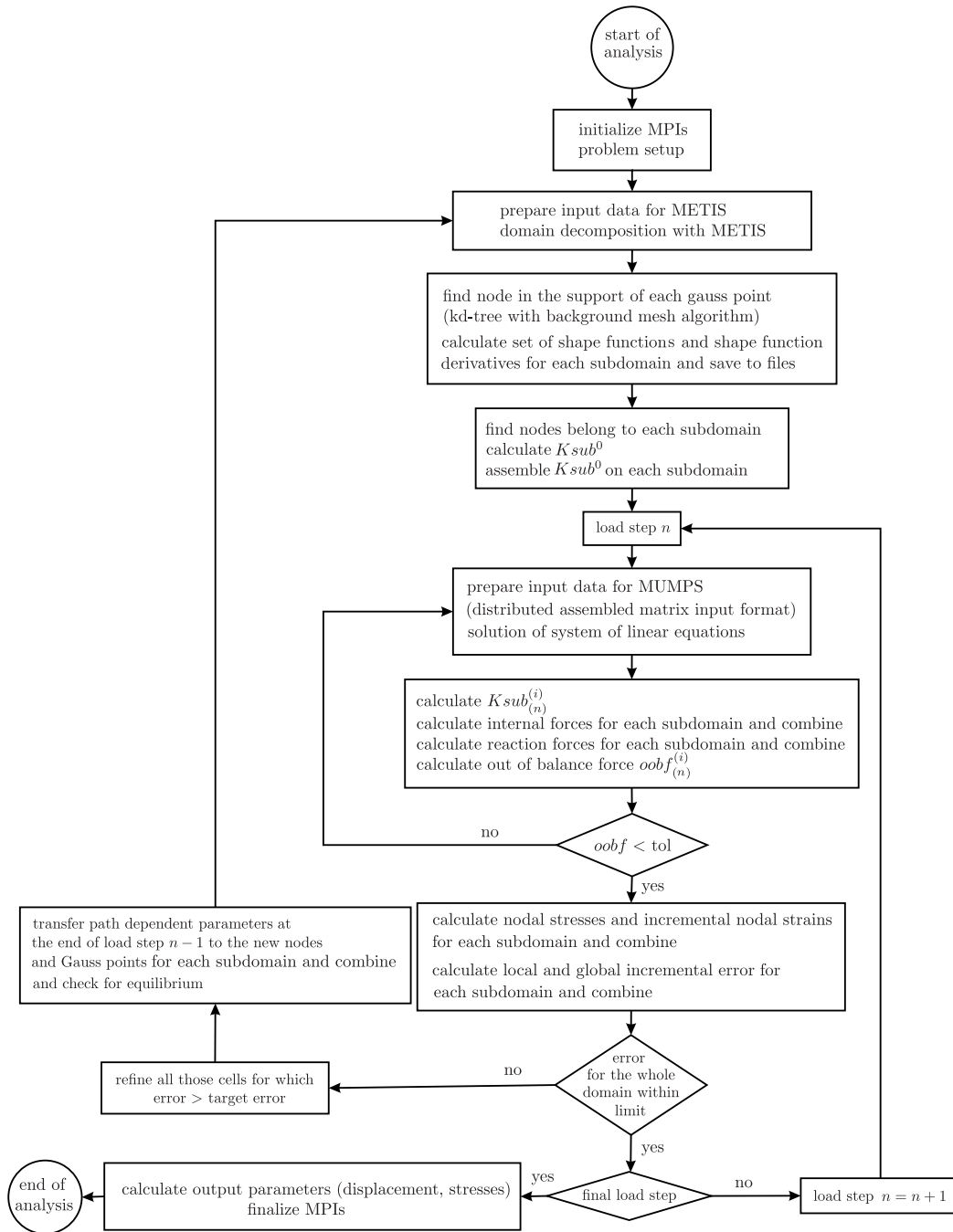


Figure 4: Nonlinear adaptive parallel algorithm

(Zienkiewicz and Zhu, 1992a) is used in the FE region of the problem domain to calculate the nodal incremental strains and stresses, a method that is difficult to parallelize. After sequential calculation of the nodal incremental strains and stresses, the error is then calculated in parallel. The rest of the algorithm is the same as described in §6, with all the relevant changes associated with the adaptively coupled FE-meshless method algorithm described in Ullah et al. (2013c).

## 8 Numerical examples

Three numerical examples are now given to demonstrate the implementation and performance of the three different parallel algorithms described in the previous sections.

### 8.1 Two-dimensional linear elastic beam problem

The first numerical example is a two-dimensional cantilever beam problem subjected to parabolic traction at the free end (Timoshenko and Goodier, 1970). The geometry, coordinate system, loading and boundary conditions for the problem, which are more complicated than is often appreciated (Augarde and Deeks, 2008), are given in Figure 5. The analytical solution for the

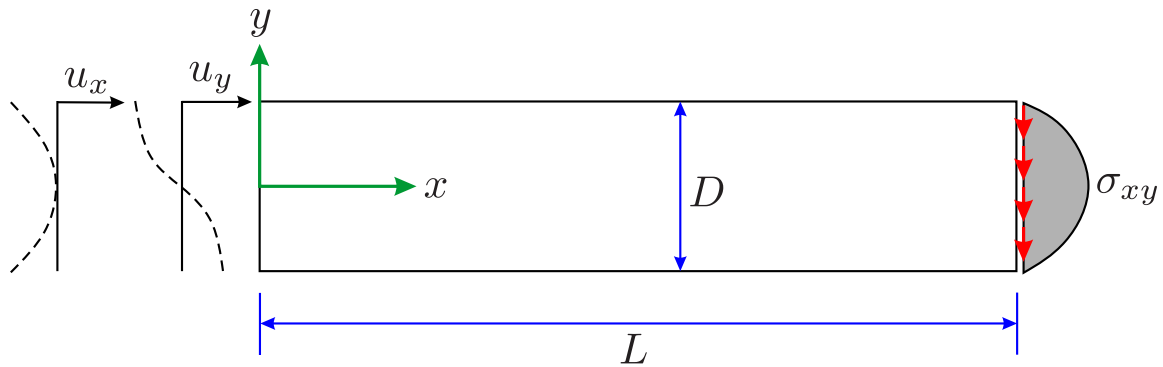


Figure 5: Geometry, boundary condition and loading for 2D beam problem

displacement field is given as (Zhuang et al., 2012b)

$$u_x(x, y) = \frac{Py}{6EI} \left[ (6L - 3x)x + (2 + \nu)y^2 - \frac{3D^2}{2}(1 + \nu) \right], \quad (15a)$$

$$u_y(x, y) = -\frac{P}{6EI} \left[ 3\nu y^2(L - x) + (3L - x)x^2 \right], \quad (15b)$$

while the analytical solution for the stress field is

$$\sigma_{xx} = \frac{P(L-x)y}{I}, \quad (16a)$$

$$\sigma_{yy} = 0, \quad (16b)$$

$$\sigma_{xy} = -\frac{P}{2I} \left[ \frac{D^2}{4} - y^2 \right], \quad (16c)$$

where  $E$  is the modulus of elasticity,  $\nu$  is the Poisson's ratio and  $I$  is the second moment of area. The problem was solved under a plane stress condition with  $P = 1000$ ,  $\nu = 0.3$ ,  $E = 30 \times 10^6$ ,  $D = 12$ ,  $L = 48$  and unit thickness, all in compatible units. Two different discretisations, coarse and fine, were used. In the fine discretisation, 6,601 nodes (DOFs=13,202) and 6,400 background cells were used, while in the coarse discretisation, nodes and background cells were decreased to 1,701 (DOFs=3,402) and 1,600 respectively.  $(4 \times 4)$  Gauss quadrature was used in each background cell and  $d_{max} = 3.0$  was used as the scaling parameter for the domain of influence. The problem was run on the Hamilton cluster with 1-25 processors. Sample METIS partitions for the fine discretisation for 2, 5, 10, 16, 20 and 25 processors are shown in Figures 6(a-f), respectively. In these figures, each color represents a separate METIS partition, for which the calculations are performed on a different processor. A comparison between the numerical and analytical displacement solution for selected nodes shown as blue circles in Figure 7(a) are shown with red crosses and black circles respectively in the same figure. Furthermore, on the neutral axis, comparison of the numerical and analytical displacement is shown in Figure 7(b). The agreement between the numerical and analytical results in this case is excellent, validating the implementation of the parallel linear elastic algorithm.

The performance indicators are shown in Figure 8. The timing results for the fine case are shown in Figure 8(a). The timings reported here for the stiffness matrix formation includes calculation of the basis functions and corresponding basis function derivatives and calculation and assembly of the stiffness matrix. The time spent on the solution of the final system of linear equations using MUMPS is tagged as "MUMPS" in Figure 8(a). The total time reported is the sum of the stiffness matrix and MUMPS times. In this problem the time spent in the solution of the system of linear equations is very small compared with the time spent in the assembly of the stiffness matrices. It is clear from Figure 8(a), that increasing the number of processors reduces all the three reported times. The timing results for the coarse case are also given in Figure 8(b) showing the same decreasing trend with increasing number of processors. A comparison between the actual speedup and ideal speedup for both the discretisations versus the number of processors is shown in 8(c). For this problem the fine discretisation performs relatively better than the coarse discretisation. For 25 processors, a speedup of 12 is obtained

for the fine discretisation, while a speedup of 9.4 is obtained for the coarse discretisation. A comparison between the actual and ideal efficiencies for both discretisations versus the number of processors is shown in Figure 8(d). For 25 processors, 48.0% and 37.6% efficiencies are recorded for fine and coarse discretisations respectively.

## 8.2 Adaptive nonlinear three-dimensional plate with a hole problem

The problem solved here is a three-dimensional plate with a hole subjected to unidirectional loading, considering both material and geometrical nonlinearities. Geometry and loading for this problem are shown in Figure 9. Due to symmetry only one-eighth of the problem (shown in gray in Figure 9). The material is modelled using a von-Mises constitutive model with the following material properties  $E = 1.0 \times 10^5$ ,  $\nu = 0.3$  and  $\sigma_y = 1.0 \times 10^3$ , all in compatible units. The problem is solved here using two different strategies: without adaptivity and with adaptivity. In the first case, all the subroutines related to adaptivity are switched off, including calculation of nodal stresses, error estimation, refinement and data transfer between the consecutive discretisations. In the following these two cases are described separately.

### 8.2.1 Without adaptivity

A total displacement of 0.15 units is applied to the top face of the plate in 15 equal steps. The scaling parameter used here for the domain of influence is  $d_{max} = 1.5$  and the problem is solved with two different discretisations (coarse with 2,793 DOFs and fine with 6,075 DOFs). The problem was run on the Hamilton cluster with 1-8 processors. Sample METIS partitions for 2, 4, 6 and 8 processors for the fine case are shown in Figures 10(a-d) respectively and for the coarse case in Figures 11(a-d). The same problem is also solved with the FEM, using a relatively fine eight-node hexahedral mesh with 18,759 DOFs to serve as a reference solution, for which the mesh is shown in Figure 12(a). A plot showing the top face reaction versus displacement for both the fine and coarse discretisations and the reference FEM is shown in Figure 12(b). They are in good agreement.

The performance indicators are shown in Figure 13. Simulation time versus the number of processors for both the discretisations are shown in Figure 13(a). The timings reported here are the total simulation times. It is clear from Figure 13(a) that for this problem with a fine discretisation, the code spends 1,008 seconds on one processor but on eight processors, it spends only 298 seconds and in the case of the coarse discretisation, it spends 277 and 91

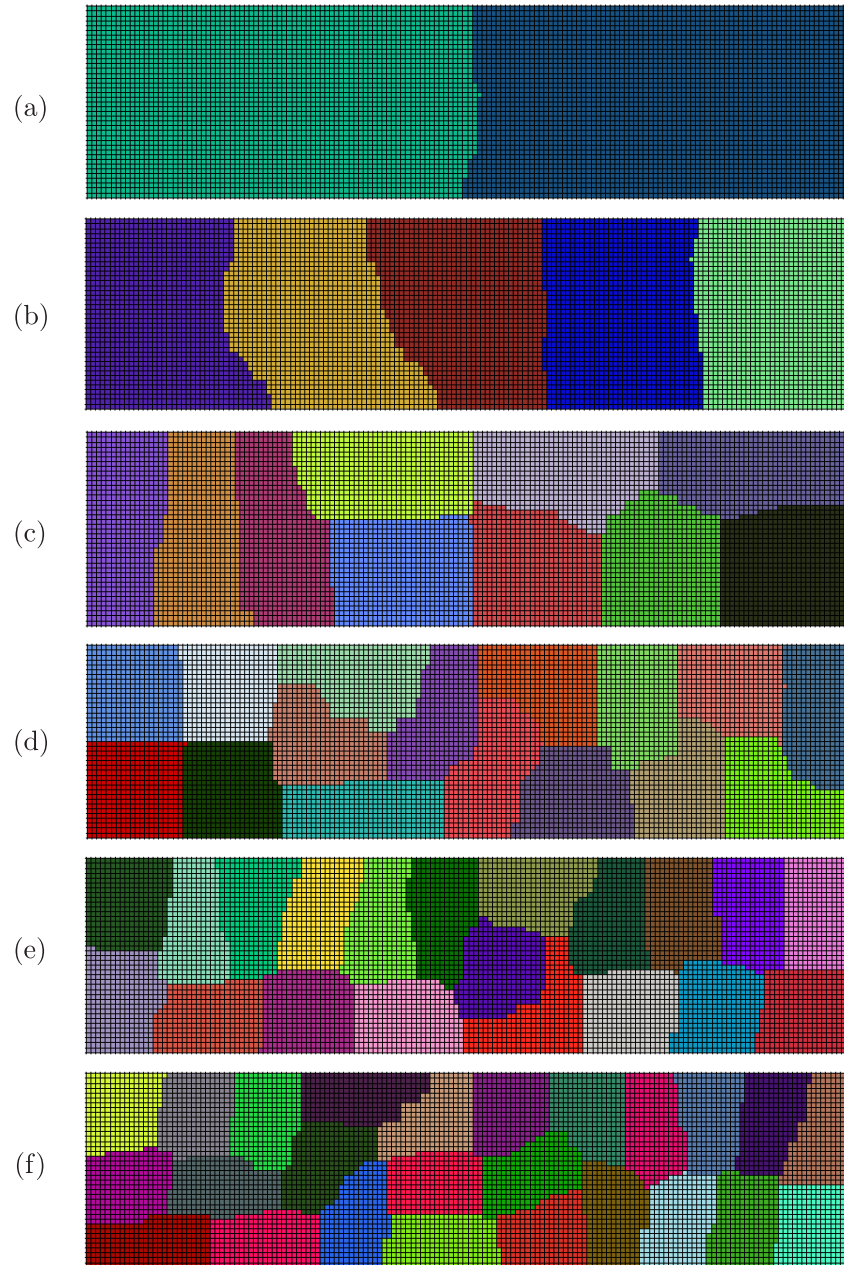


Figure 6: Selective METIS partitions for the discretisation with 13202 DOFs for the two-dimensional beam problem

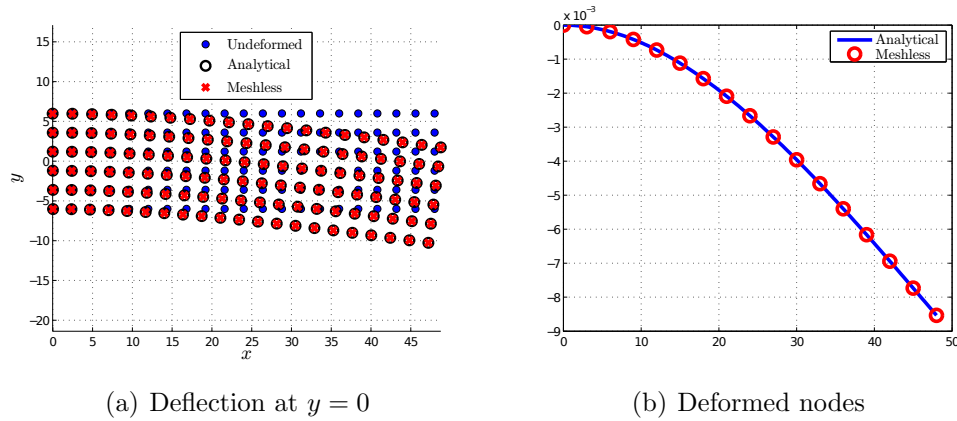


Figure 7: Deflections for the selective nodes for the two-dimensional beam problem

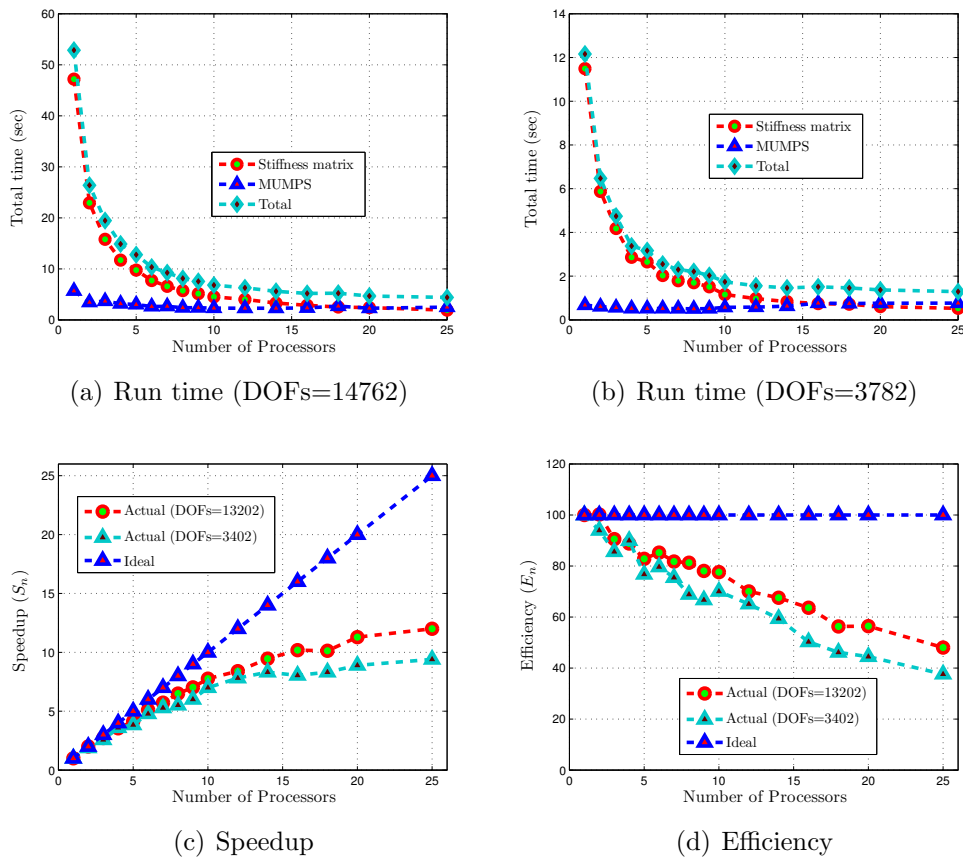


Figure 8: Performance on the Hamilton cluster using 1-25 processors for the two-dimensional beam problem



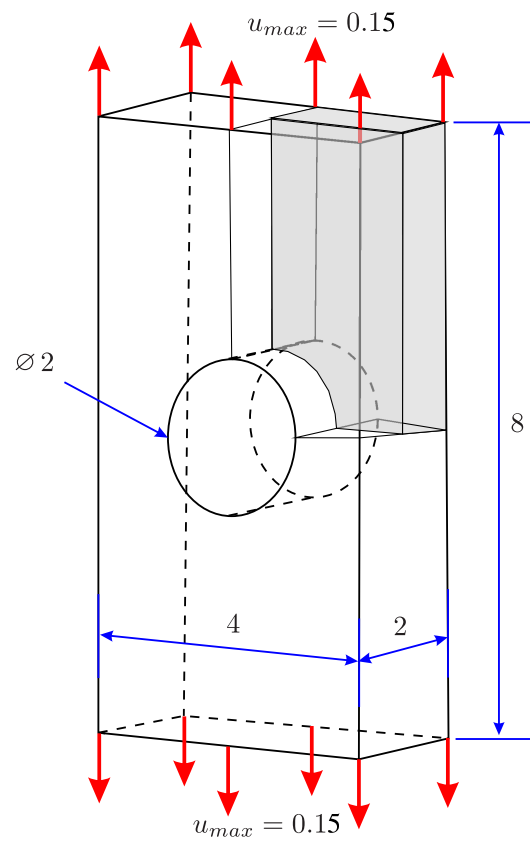


Figure 9: Geometry, boundary condition and loading for the 3D plate with a hole problem

seconds on one and eight processors respectively, a significant reduction in simulation time. A comparison between the actual speedup versus the number of processors for both discretisations and the ideal speedup is shown in Figure 13(b). For eight processors speedups of 3.38 and 3.04 are obtained for the fine and coarse discretisations respectively. A comparison between the efficiencies for both discretisations and the ideal is shown in Figure 13(c). For eight processors 42.26% and 37.95% efficiencies are obtained for the fine and coarse discretisations respectively.

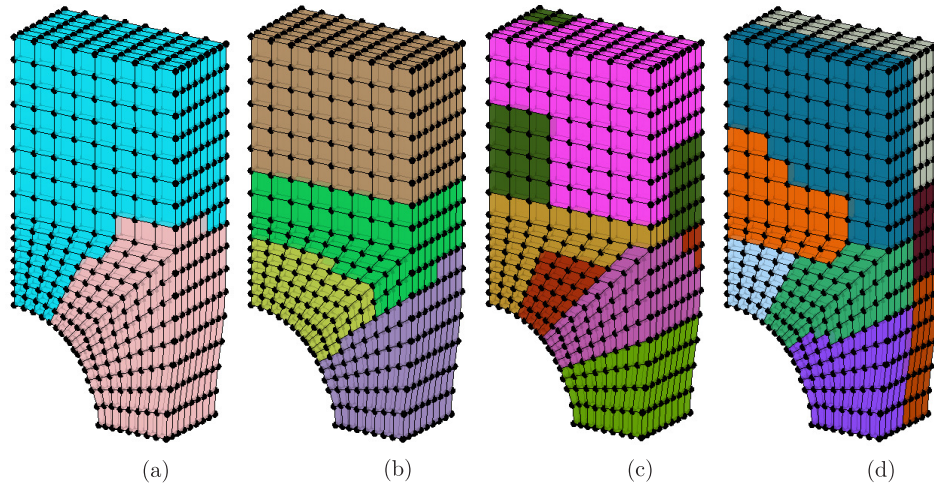


Figure 10: Selective METIS partitions for 6075 degrees of freedom for the 3D plate with a hole problem

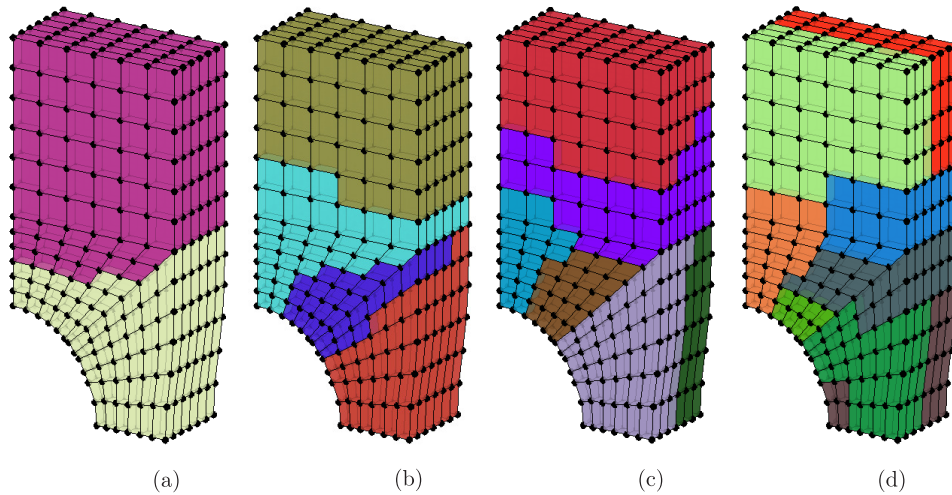


Figure 11: Selective METIS partitions for 2,793 degrees of freedom for the 3D plate with a hole problem

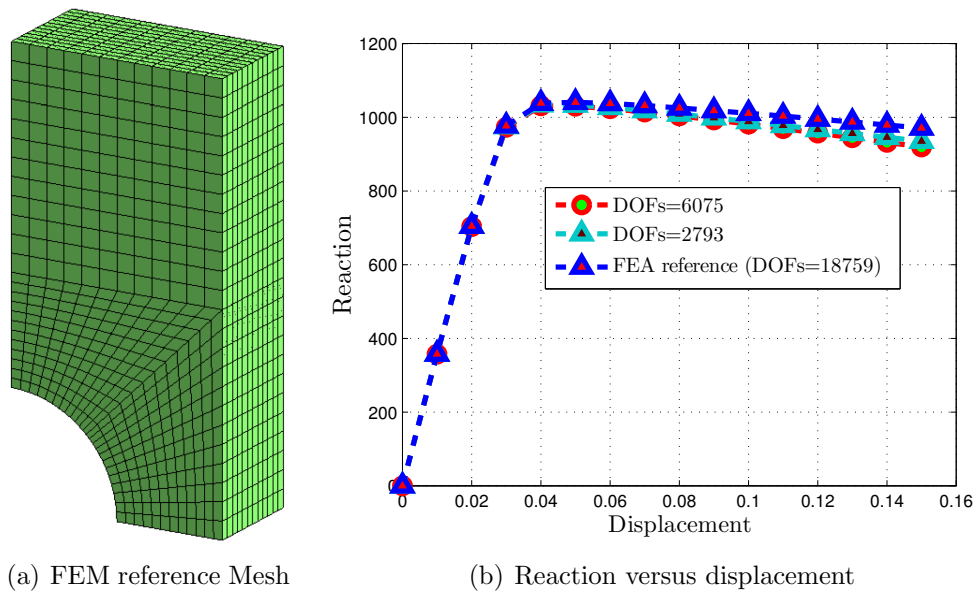


Figure 12: FEM reference mesh and reaction versus displacement for the 3D plate with a hole problem

### 8.2.2 With adaptivity

In the adaptive case, a total displacement of 0.5 units was applied to the top face of the plate in 20 equal steps. The scaling parameters for the analysis and projection domains of influence were  $d_{max}^a = 1.5$  and  $d_{max}^p = 1.1$  respectively. A relative error of 15% was permitted in the analysis. A very coarse discretisation was used at the start of the analysis with only 189 DOFs, which was subsequently adaptively refined and the number of DOFs in the second and third discretisations was 852 and 3,486 respectively. This problem was run on the Hamilton cluster using 1-6 processors. The maximum number of processors was restricted here by the coarse initial discretisation, as METIS cannot divide the mesh into more than six subdomains. Sample METIS partitions of the adaptively refined discretisations for two processors are shown in Figures 14(a-c), while the final deformed configuration is shown in Figure 14(d). The same METIS partitions and the final deformed configuration in the case of five processors are shown in Figures 15(a-d). The number of processors was kept constant during the analysis and specified at the start of simulation. METIS repartitions the problem domain into the same number of subdomains as processors after each refinement. The final displacement contours in the  $x$  and  $y$  directions over the full plate are shown in Figures 16(a) and 16(b) respectively. Necking of the centre of the plate is obvious in both figures. The same problem was also solved with the same FEM reference mesh as in the previous section (see Figure 12(a)). A comparison

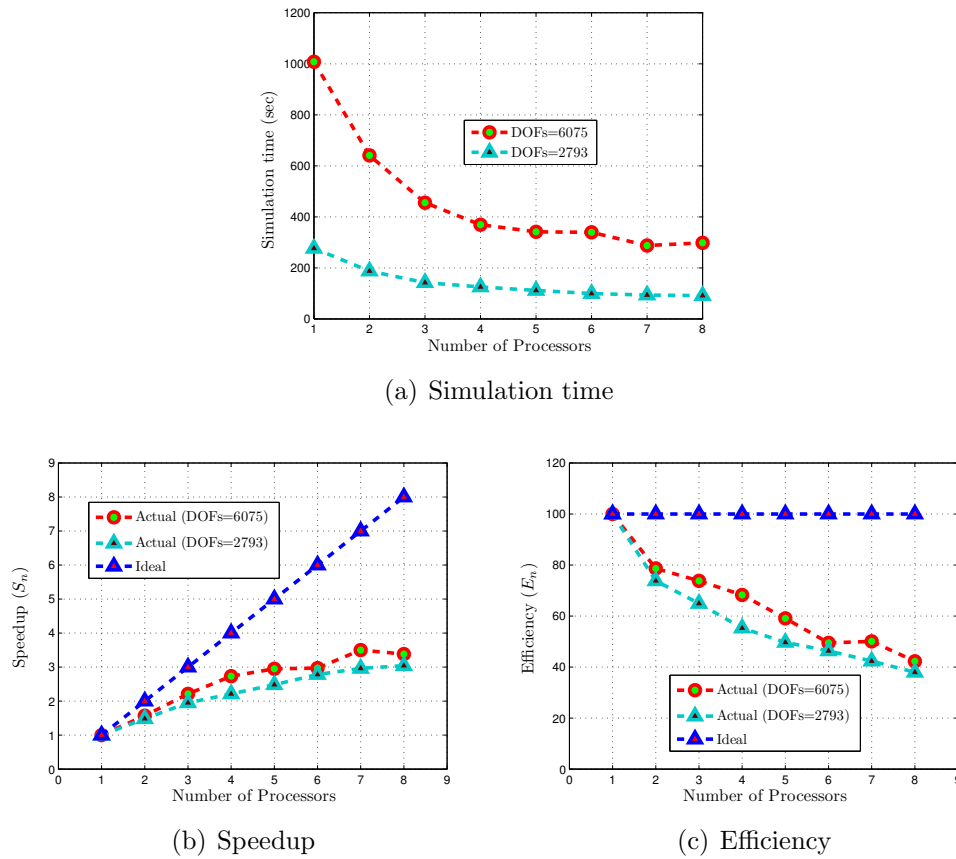


Figure 13: Performance on the Hamilton cluster using 1-8 processors for the the 3D plate with a hole problem

of the top face reaction versus displacement for this problem with the reference FEM solution is shown in Figure 16(c). The jumps in the adaptive load-displacement path represent points where rediscritisation is taking place and mapping has been carried out. The jumps are due to changes in the equilibrium state of the domain due to the altered discretisation. These plots show results from successive analyses, not a single calculation.

Performances indicators of the method run on the Hamilton cluster are shown in Figure 17. Simulation time against the number of processors is shown in Figure 17(a). The timings reported here are full simulation times. On one processor, simulation took 614 seconds, while for six processors, the simulation took 190 seconds. Comparisons of speedup and efficiency with the corresponding ideal values are given in Figures 17(b) and 17(c). In the case of six processors speedup and efficiency achieved were 3.23 and 53.76% respectively.

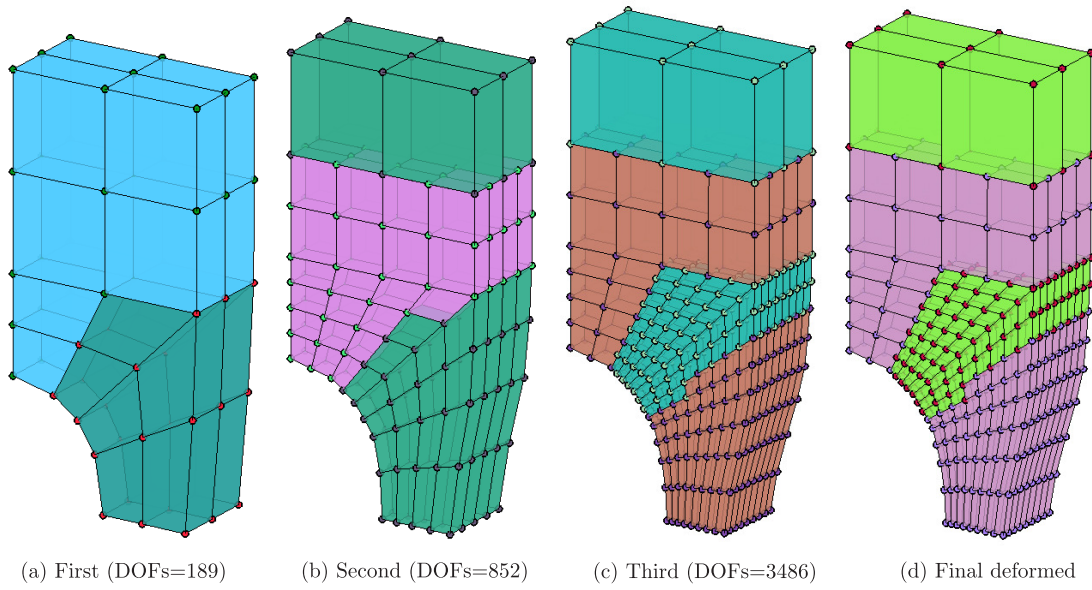


Figure 14: Step by step METIS partitions for two processors for the adaptive 3D plate with a hole problem

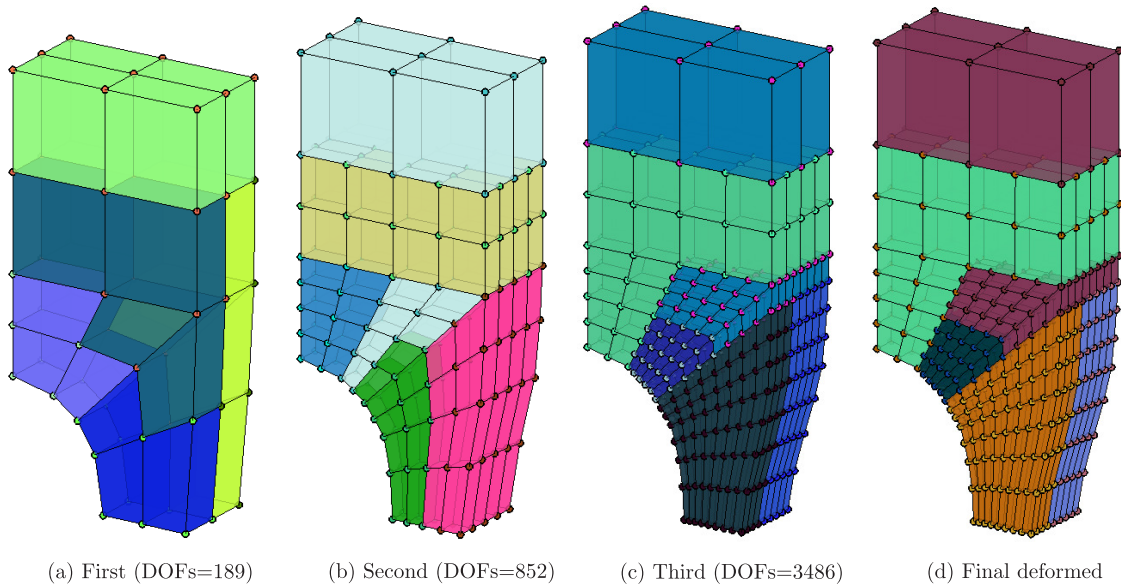


Figure 15: Step by step METIS partitions for five processors for the adaptive 3D plate with a hole problem

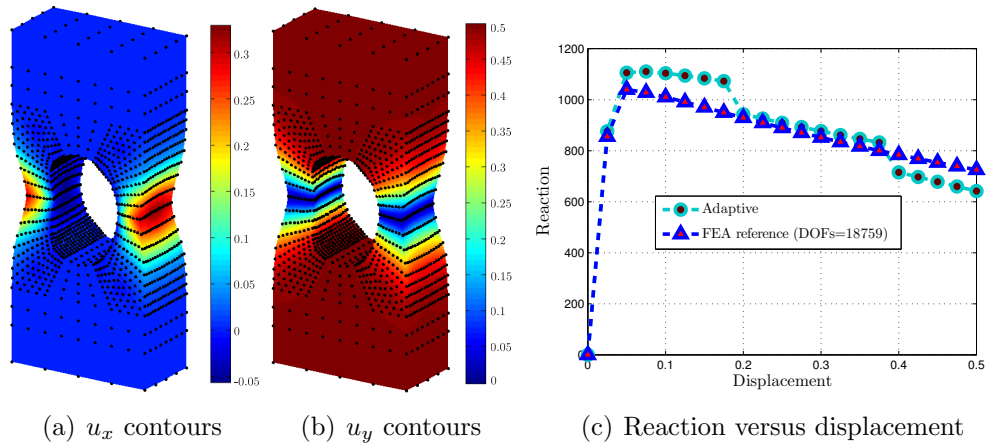


Figure 16: Final displacements and reaction versus displacement for the adaptive 3D plate with a hole problem

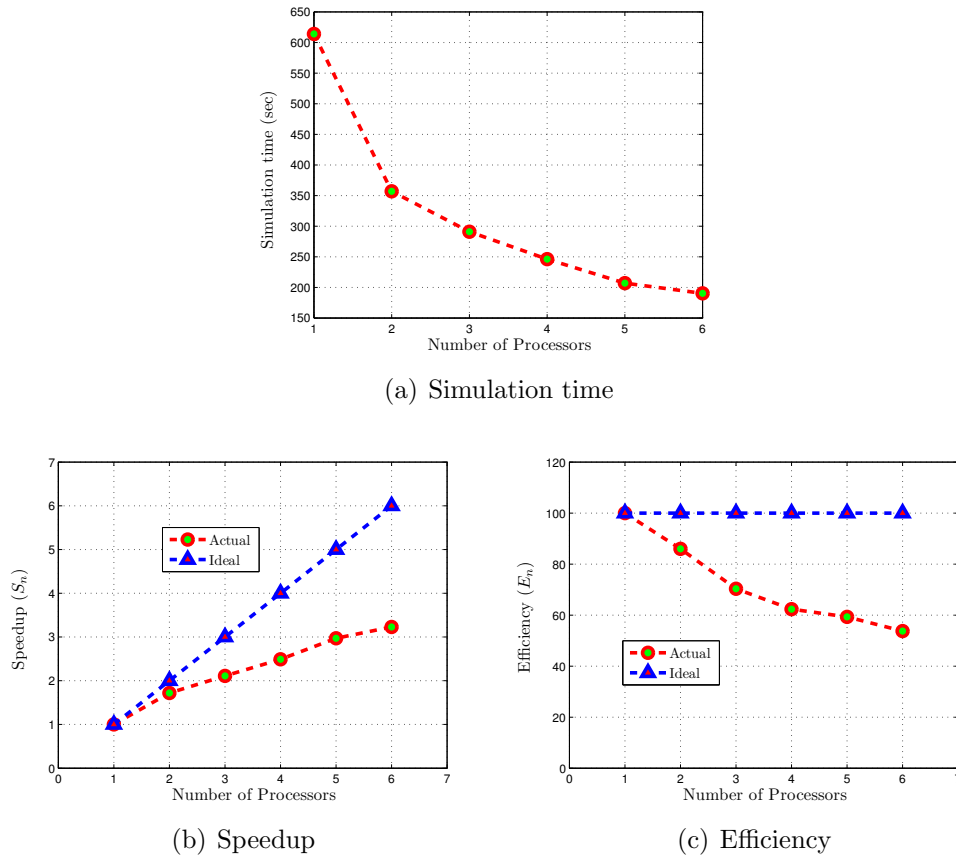


Figure 17: Performances on the Hamilton cluster using 1-6 processors for the adaptive 3D plate with a hole problem



### 8.3 Adaptively coupled nonlinear three-dimensional plate with a hole problem

The same problem as used in the previous section was solved with the parallel nonlinear adaptively coupled FE-meshless method code. Again only one-eighth of the problem was modelled and a total displacement of 1.5 units was applied to the top face of the plate in 60 steps. Scaling parameters used for the domains of influence of analysis and projections were  $d_{max}^a = 1.5$  and  $d_{max}^p = 1.1$  respectively and the permissible relative error was 15%. The problem was first analysed using a FE mesh with 6,075 DOFs as shown in Figure 18(a). During the analysis, those FEs which violated a specified error measure, based on the Zienkiewicz & Zhu error estimation procedure, were converted into a meshless method zone. The second discretisation, or the first coupled FE-meshless method discretisation, is shown in Figure 18(b). During this first conversion, the number of degrees of freedom remained the same. The third (21609 DOFs) and fourth (52386 DOFs) discretisations are shown in Figures 18(c) and 18(d) respectively, which were obtained from adaptive refinement based on the combined Zienkiewicz & Zhu and Chung & Belytschko error estimations. Contours of  $u_x$  and  $u_y$  on the final deformed configurations are shown in Figures 19(b) and 19(c) respectively. For comparison, the original undeformed configuration is also shown in Figure 19(a). Top face reaction versus displacement is shown in Figure 22. The path for this case is tagged as “adaptive”. This problem was solved on the Hamilton cluster using 50 processors with a total simulation time of 9,391 seconds. It is clear from Figures 19 and 22, that the developed algorithm, can efficiently handle very large deformation problems.

For comparison, the same problem was also solved with the FEM, with eight-node hexahedral elements using three different meshes as shown in Figures 20(a-c). The first mesh is very coarse with only 975 DOFs, the second one is relatively fine with 42,483 DOFs and the third one is very fine with 154,128 DOFs. For the coarse case, the analysis was run on the Hamilton cluster using 10 processors, and the total simulation time was 242 seconds. The final deformed configuration for the full plate with  $u_y$  contours is shown in Figure 21(a). In this case, due to volumetric locking, material on both sides of the hole moves rigidly towards the centre of the hole. Although, some necking can be seen near the centre of the hole, it is less obvious as compared to the previous adaptively coupled FE-meshless method case. The top face reaction versus displacement path for this case is shown in Figure 22, tagged as “FEA (DOFs=975)”. Although, some geometric softening can be seen in this case, the response is very rigid as compared to the adaptively coupled FE-meshless method cases, and is unrealistic. For the second and third FE meshes, the final deformed configurations with  $u_y$  contours are shown in Figures 21(b) and 21(c) respectively. In the fine FEM case, the analysis was run on the



Hamilton cluster using 40 processors with 100 load steps, with a total simulation time of 14,579 seconds. In the very fine FEM case, the analysis was run on the Hamilton cluster on 100 processors with 50 load steps, with a total simulation time of 48,680 seconds.

In Figure 21(b), necking is more prominent and rigid material movement toward the centre of the hole is less obvious as compared to the response of the coarse FEM model, shown in Figure 21(a). For the very fine FEM case shown in Figure 21(c), the response is even better than that shown in Figure 21(b) with very prominent necking as one would expect physically, and almost no rigid material movement near the centre of the hole. The top face reaction versus displacement curve for the second and third FEM cases are also shown in Figure 22, which are tagged as “FEA (DOFs=42,483)” and “FEA (DOFs=154,128)” respectively. These reaction versus displacement curves show more geometric softening as compared to the coarse FEM discretisation.

A summary of the results for this final demonstration problem, with four different discretisations, is given in Table 2. Due to the use of different load steps and numbers of processors for each analysis, work done per load step is calculated for each analysis as

$$\text{Work done per load step} = \frac{\text{Run time} \times \text{No of processors}}{\text{Load steps}}, \quad (17)$$

and is also given in the table for comparison. As compared to the fine FEA case, work done per load step associated with the adaptive case is very small. Work done per load step associated with the first two FEA cases is also very small, but as shown above in these cases the results are not realistic.

Cases	DoFs			Load steps	Number of processors used	Run time (sec)	Work per load step
Adaptive-1	6,075	21,609	52,386	60	50	9,391	7825.8
FEA-1	975			100	10	242	24.2
FEA-2	42,483			100	40	14,579	5831.6
FEA-3	154,128			50	100	48,680	97360

Table 2: Results summary for the adaptively coupled nonlinear three-dimensional plate with a hole problem

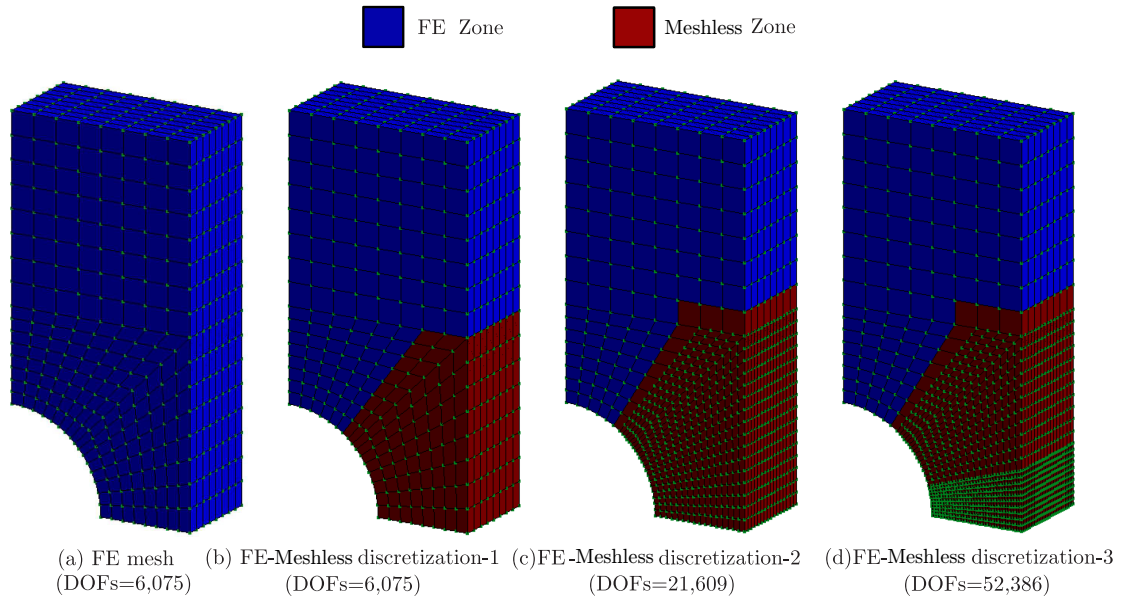


Figure 18: Step by step discretisations for the “adaptive” case for the final demonstration problem

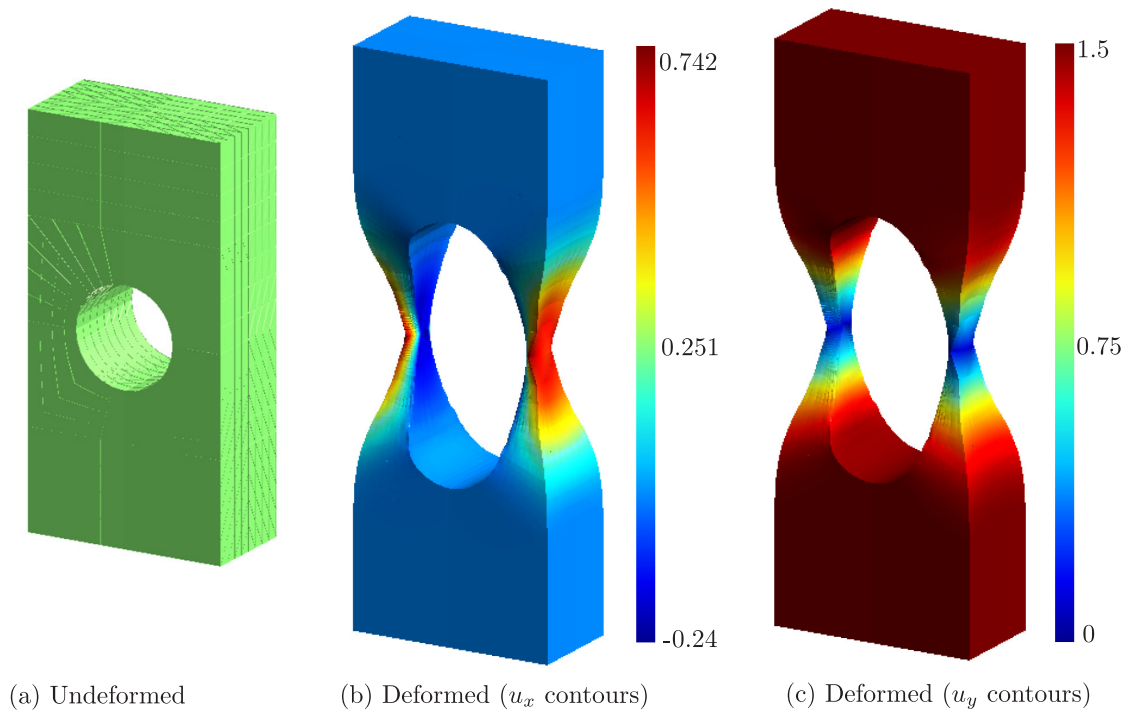


Figure 19: Contours of  $u_x$  and  $u_y$  over the final deformed geometry for the “adaptive” case for the adaptively coupled nonlinear three-dimensional plate with a hole problem

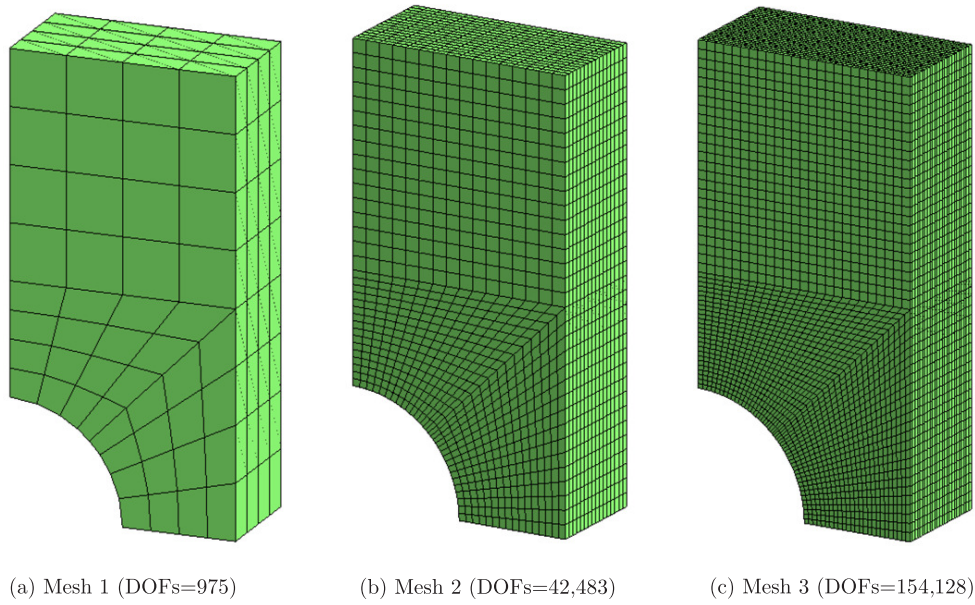


Figure 20: Reference FEM meshes for the adaptively coupled nonlinear three-dimensional plate with a hole problem

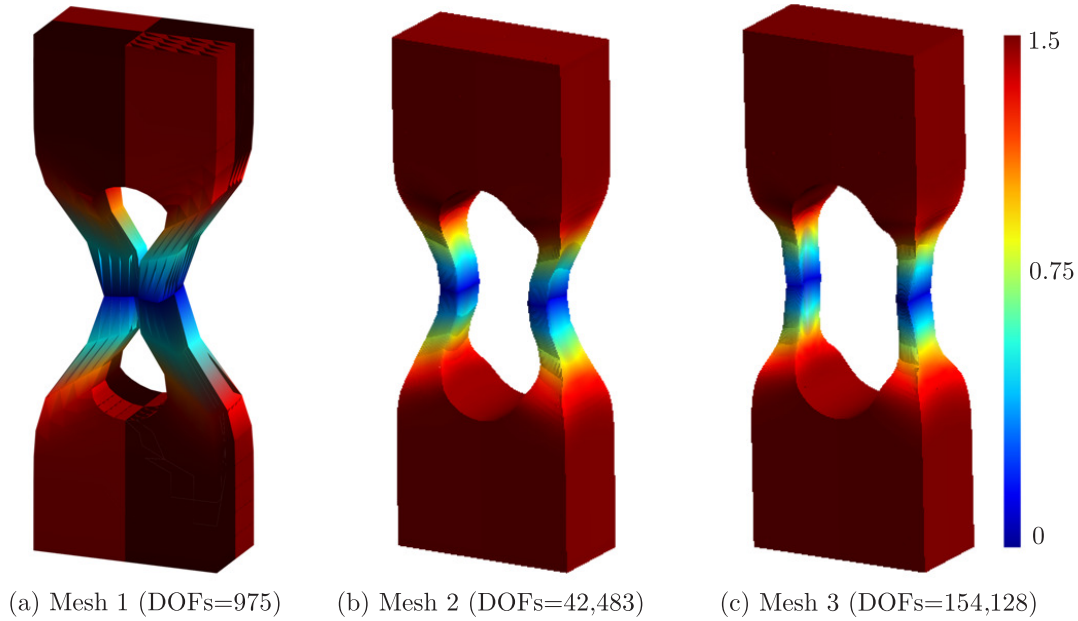


Figure 21: Contours of  $u_y$  over the final deformed geometry for the reference FEM meshes for the adaptively coupled nonlinear three-dimensional plate with a hole problem

## 9 Concluding remarks

Meshless methods are of considerable interest in the computational mechanics community at present, however it is recognised that they can be computationally inefficient. In this paper

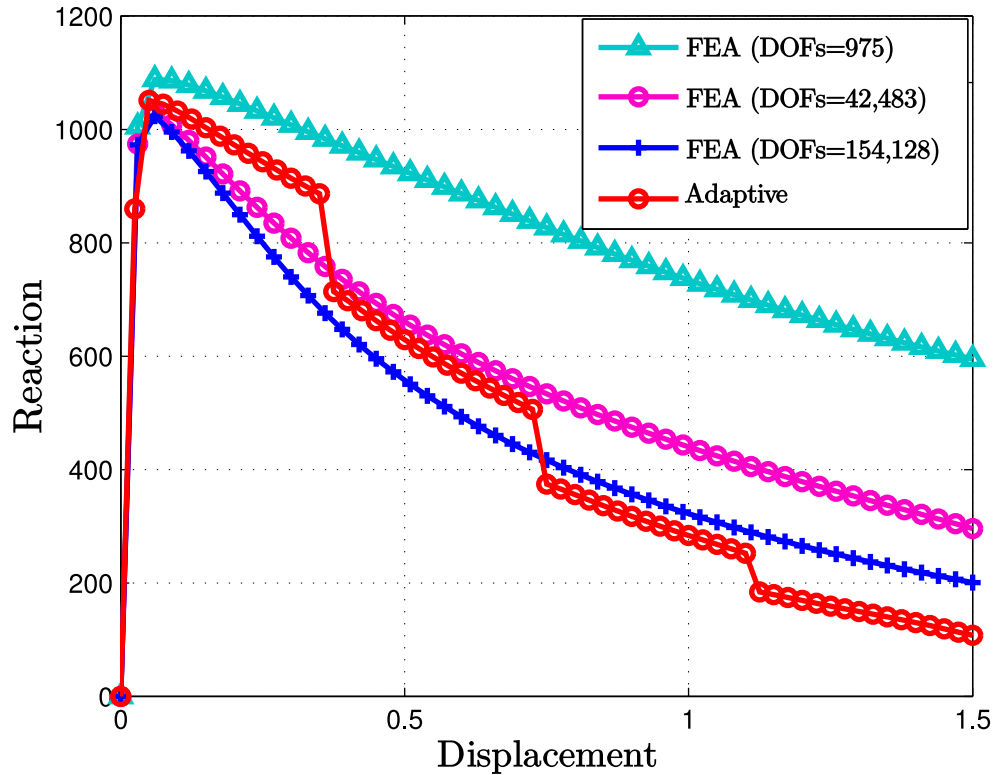


Figure 22: Reaction versus displacement for the adaptively coupled nonlinear three-dimensional plate with a hole problem

parallel algorithms for distributed memory computer architectures have been presented for a linear and adaptive nonlinear meshless method (the EFGM with max-ent basis functions). The method has then been extended to the case of a coupled adaptive FE-meshless method. A number of numerical examples have demonstrated the accuracy and efficiency of the methods on some challenging nonlinear problems.

## Acknowledgements

The first author was supported by an Overseas Research Students Awards Scheme award from Durham University during the research which led to this paper.

## References

- Amiri, F., Anitescu, C., Arroyo, M., Bordas, S., and Rabczuk, T. (2014)a, “XLME interpolants, a seamless bridge between XFEM and enriched meshless methods”. *Computational Mechanics*, 53(1):45–57.
- Amiri, F., Millán, D., Shen, Y., Rabczuk, T., and Arroyo, M. (2014)b, “Phase-field modeling of fracture in linear thin shells”. *Theoretical and Applied Fracture Mechanics*, 69:102 – 109.
- Arroyo, M. and Ortiz, M. (2006), “Local *maximum-entropy* approximation schemes: a seamless bridge between finite elements and meshfree methods”. *International Journal for Numerical Methods in Engineering*, 65:2167–2202.
- Augarde, C. E. and Deeks, A. J. (2008), “The use of Timoshenko’s exact solution for a cantilever beam in adaptive analysis”. *Finite Elements in Analysis and Design*, 44:595 – 601.
- Barbieri, E. and Meo, M. (2012), “A fast object-oriented Matlab implementation of the Reproducing Kernel Particle Method”. *Computational Mechanics*, 49:581–602.
- Becene, A. T. (2003), *Parallel processing of finite strain, materially nonlinear and incompressible finite element analysis problems*. PhD thesis, University of Rochester.
- Belytschko, T., Lu, Y. Y., and Gu, L. (1994), “Element-free Galerkin methods”. *International Journal for Numerical Methods in Engineering*, 37:229–256.
- Belytschko, T., Organ, D., and Krongauz, Y. (1995), “A coupled finite element-element-free Galerkin method”. *Computational Mechanics*, 17:186–195.
- Belytschko, T., Krongauz, Y., Dolbow, J., and Gerlach, C. (1998), “On the completeness of meshfree particle methods”. *International Journal for Numerical Methods in Engineering*, 43(5):785–819.
- Boroomand, B. and Zienkiewicz, O. C. (1999), “Recovery procedures in error estimation and adaptivity. Part II: Adaptivity in nonlinear problems of elasto-plasticity behaviour”. *Computer Methods in Applied Mechanics and Engineering*, 176(1-4):127 – 146.
- Cai, Y., Zhu, H., and Zhuang, X. (2013), “A continuous/discontinuous deformation analysis (CDDA) method based on deformable blocks for fracture modeling”. *Frontiers of Structural and Civil Engineering*, 7(4):369–378.
- Carter, W. T., Sham, T. L., and Law, K. H. (1989), “A parallel finite element method and its prototype implementation on a hypercube”. *Computers & Structures*, 31(6):921 – 934.

- Chiang, K. N. and Fulton, R. E. (1990), “Concepts and implementation of parallel finite element analysis”. *Computers & Structures*, 36(6):1039 – 1046.
- Chung, H. J. and Belytschko, T. (1998), “An error estimate in the EFG method”. *Computational Mechanics*, 21:91–100.
- Cormen, T., Leiserson, C., Rivest, R., and Stein, C. (2009), *Introduction to algorithms*. MIT Press, Cambridge, 3rd edition.
- Danielson, K. T., Hao, S., Liu, W. K., Uras, R. A., and Li, S. (2000), “Parallel computation of meshless methods for explicit dynamic analysis”. *International Journal for Numerical Methods in Engineering*, 47(7):1323–1341.
- Farhat, C. and Roux, F. X. (1991), “A method of finite element tearing and interconnecting and its parallel solution algorithm”. *International Journal for Numerical Methods in Engineering*, 32(6):1205–1227.
- Fernández-Méndez, S. and Huerta, A. (2000), “Enrichment and coupling of the finite element and meshless methods”. *International Journal for Numerical Methods in Engineering*, 48: 1615–1636.
- Gropp, W., Huss-Lederman, S., Lumsdaine, A., Lusk, E., Nitzberg, B., Saphir, W., and Snir, M. (1998), *MPI: The Complete Reference-Volume 2: The MPI2 Extensions*. MIT, Cambridge, MA, USA.
- Gropp, W., Lusk, E., and Skjellum, A. (1999)a, *Using MPI: Portable Parallel Programming with the Message-Passing Interface*. MIT Press, Cambridge, MA, USA, 2nd edition.
- Gropp, W., Lusk, E., and Thakur, R. (1999)b, *Using MPI-2: Advanced Features of the Message-Passing Interface*. MIT Press, Cambridge, MA, USA.
- Grosso, A. D. and Righetti, G. (1988), “Finite element techniques and artificial intelligence on parallel machines”. *Computers & Structures*, 30(4):999 – 1007.
- Gu, Y. T. and Zhang, L. C. (2008), “Coupling of the meshfree and finite element methods for determination of the crack tip fields”. *Engineering Fracture Mechanics*, 75(5):986 – 1004.
- Günther, F., Liu, W. K., Diachin, D., and Christon, M. A. (2000), “Multi-scale meshfree parallel computations for viscous, compressible flows”. *Computer Methods in Applied Mechanics and Engineering*, 190:279 – 303.
- Hegen, D. (1996), “Element-free Galerkin methods in combination with finite element approaches”. *Computer Methods in Applied Mechanics and Engineering*, 135(1-2):143 – 166.



- Hu, W., Yao, L. G., and Hua, Z. Z. (2007), “Parallel point interpolation method for three-dimensional metal forming simulations”. *Engineering Analysis with Boundary Elements*, 31(4):326 – 342.
- Huerta, A., Fernández-Méndez, S., and Liu, W. K. (2004), “A comparison of two formulations to blend finite elements and mesh-free methods”. *Computer Methods in Applied Mechanics and Engineering*, 193:1105 – 1117.
- Jones, M. T. and Plassmann, P. E. (1994), “Computational results for parallel unstructured mesh computations”. *Computing Systems in Engineering*, 5:297 – 309.
- Karypis, G. (August 2011), *METIS: A Software Package for Partitioning Unstructured Graphs, Partitioning Meshes, and Computing Fill-Reducing Orderings of Sparse Matrices Version 5.0*. Department of Computer Science & Engineering, University of Minnesota, Minneapolis, MN 55455. Available at:<http://glaros.dtc.umn.edu/gkhome/metis/metis/overview> (Accessed date: 26 Jan 2013).
- Karypis, G. and Kumar, V. (1998), “A Fast and High Quality Multilevel Scheme for Partitioning Irregular Graphs”. *SIAM Journal on Scientific Computing*, 20(1):359–392.
- Kennel, M. B. KDTree 2: Fortran 95 and C++ software to efficiently search for near neighbors in a multi-dimensional Euclidean space, (2004).
- Leland, R. and Hendrickson, B. (1995), *The Chaco user’s guide: version 2.0*. Sandia National Labs, Albuquerque, NM. Technical Report SAND94-2692.
- Liu, W. K., Jun, S., and Zhang, Y. F. (1995), “Reproducing kernel particle methods”. *International Journal for Numerical Methods in Fluids*, 20(8-9):1081–1106.
- Luo, J. C. and Friedman, M. B. (1990), “A parallel computational model for the finite element method on a memory-sharing multiprocessor computer”. *Computer Methods in Applied Mechanics and Engineering*, 84(2):193 – 209.
- Medina, D. F. and Chen, J. K. (2000), “Three-dimensional simulations of impact induced damage in composite structures using the parallelized SPH method”. *Composites Part A: Applied Science and Manufacturing*, 31(8):853 – 860.
- Metsis, P. and Papadrakakis, M. (2012), “Overlapping and non-overlapping domain decomposition methods for large-scale meshless EFG simulations”. *Computer Methods in Applied Mechanics and Engineering*, 229 - 232(0):128 – 141.



- Millán, D., Rosolen, A., and Arroyo, M. (2011), “Thin shell analysis from scattered points with maximum-entropy approximants”. *International Journal for Numerical Methods in Engineering*, 85(6):723–751.
- Millán, D., Sukumar, N., and Arroyo, M. (2015), “Cell-based maximum-entropy approximants”. *Computer Methods in Applied Mechanics and Engineering*, 284:712–731.
- Moore, A. (1991), A tutorial on kd-trees. Technical Report 209, University of Cambridge Computer Laboratory. Extract from PhD thesis.
- MUMPS. (May 2011), *MUltifrontal Massively Parallel Solver - (MUMPS 4.10.0) Users’ Guide*. Available at: <http://graal.ens-lyon.fr/MUMPS/> (Accessed date: 26 Jan 2013).
- Nguyen-Thanh, N., Valizadeh, N., Nguyen, M., Nguyen-Xuan, H., Zhuang, X., Areias, P., Zi, G., Bazilevs, Y., Lorenzis, L. D., and Rabczuk, T. (2015), “An extended isogeometric thin shell analysis based on Kirchhoff–Love theory”. *Computer Methods in Applied Mechanics and Engineering*, 284:265 – 291. Isogeometric Analysis Special Issue.
- Ortiz, A., Puso, M., and Sukumar, N. (2010), “Maximum-entropy meshfree method for compressible and near-incompressible elasticity”. *Computer Methods in Applied Mechanics and Engineering*, 199(25-28):1859 – 1871.
- Ortiz, A., Puso, M., and Sukumar, N. (2011), “Maximum-entropy meshfree method for incompressible media problems”. *Finite Elements in Analysis and Design*, 47(6):572 – 585.
- Pacheco, P. (2011), *An Introduction to Parallel Programming*. Elsevier Inc.
- Pacheco, P. S. (1997), *Parallel Programming with MPI*. Morgan Kaufmann Publishers, Inc.
- Peco, C., Millán, D., Rosolen, A., and Arroyo, M. (2015), “Efficient implementation of Galerkin meshfree methods for large-scale problems with an emphasis on maximum entropy approximants”. *Computers & Structures*, 150:52–62.
- Quaranta, G., Kunnath, S., and Sukumar, N. (2012), “Maximum-entropy meshfree method for nonlinear static analysis of planar reinforced concrete structures”. *Engineering Structures*, 42:179 – 189.
- Rabczuk, T. and Belytschko, T. (2005), “Adaptivity for structured meshfree particle methods in 2D and 3D”. *International Journal for Numerical Methods in Engineering*, 63(11):1559–1582.
- Rabczuk, T. and Belytschko, T. (2006), “Application of Particle Methods to Static Fracture of Reinforced Concrete Structures”. *International Journal of Fracture*, 137:19–49.

- Rabczuk, T. and Belytschko, T. (2007), “A three-dimensional large deformation meshfree method for arbitrary evolving cracks”. *Computer Methods in Applied Mechanics and Engineering*, 196(29–30):2777 – 2799.
- Rabczuk, T. and Eibl, J. (2003), “Simulation of high velocity concrete fragmentation using SPH/MLSPH”. *International Journal for Numerical Methods in Engineering*, 56(10):1421–1444.
- Rabczuk, T. and Samaniego, E. (2008), “Discontinuous modelling of shear bands using adaptive meshfree methods”. *Computer Methods in Applied Mechanics and Engineering*, 197(6–8):641 – 658.
- Rabczuk, T., Xiao, S. P., and Sauer, M. (2006), “Coupling of mesh-free methods with finite elements: basic concepts and test results”. *Communications in Numerical Methods in Engineering*, 22(10):1031–1065.
- Rao, B. and Rahman, S. (2001), “A coupled meshless-finite element method for fracture analysis of cracks”. *International Journal of Pressure Vessels and Piping*, 78(9):647 – 657.
- Rauber, T. and Rünger, G. (2010), *Parallel Programming for Multicore and Cluster Systems*. Springer, 1st edition.
- Rosolen, A. and Arroyo, M. (2013), “Blending isogeometric analysis and local maximum entropy meshfree approximants”. *Computer Methods in Applied Mechanics and Engineering*, 264:95 – 107.
- Rosolen, A., Millán, D., and Arroyo, M. (2012), “Second-order convex maximum entropy approximants with applications to high-order PDE”. *International Journal for Numerical Methods in Engineering*, pages n/a–n/a.
- Rycroft, C. H. (2007), *Multiscale modeling in granular flow*. PhD thesis, Massachusetts Institute of Technology.
- Rycroft, C. H., Grest, G. S., Landry, J. W., and Bazant, M. Z. (2006), “Analysis of granular flow in a pebble-bed nuclear reactor”. *Physical Review E*, 74 (2):021306.
- Shirazaki, M. and Yagawa, G. (1999), “Large-scale parallel flow analysis based on free mesh method: a virtually meshless method”. *Computer Methods in Applied Mechanics and Engineering*, 174:419 – 431.
- Singh, I. V. and Jain, P. K. (2005), “Parallel EFG algorithm for heat transfer problems”. *Advances in Engineering Software*, 36(8):554 – 560.

- Slim, H. An introduction to parallel programming, Guide 48, Version: 2.0. Durham University (Available at: <https://www.dur.ac.uk/resources/its/info/guides/48ParallelProg.pdf>), (10 2010), (Accessed date: 2 Jan 2013).
- Snir, M., Otto, S., Huss-Lederman, S., Walker, D., and Dongarra, J. (1998), *MPI-The Complete Reference, Volume 1: The MPI Core*. MIT Press, Cambridge, MA, USA, 2nd. (revised) edition. ISBN 0262692155.
- Sukumar, N. (2004), “Construction of polygonal interpolants: a maximum entropy approach”. *International Journal for Numerical Methods in Engineering*, 61:2159–2181.
- Sukumar, N. and Wright, R. W. (2007), “Overview and construction of meshfree basis functions: from moving least squares to entropy approximants”. *International Journal for Numerical Methods in Engineering*, 70:181–205.
- Timoshenko, S. P. and Goodier, J. N. (1970), *Theory of Elasticity*. McGraw-Hill, New York.
- Ullah, Z. (2013), *Nonlinear solid mechanics analysis using the parallel selective element-free Galerkin method*. PhD thesis, School of Engineering & Computing Sciences, Durham University, United Kingdom.
- Ullah, Z. and Augarde, C. E. Solution of elasto-statics problems using the element-free galerkin method with local maximum entropy shape functions. In *18<sup>th</sup> UK Conference of the Association for Computational Mechanics in Engineering (ACME), Southampton University, Southampton, UK*, pages 161–164, (2010).
- Ullah, Z. and Augarde, C. E. (2013), “Finite deformation elasto-plastic modelling using an adaptive meshless method”. *Computers & Structures*, 118:39–52.
- Ullah, Z., Augarde, C. E., Crouch, R. S., and Coombs, W. M. FE-EFGM coupling using maximum entropy shape functions and its application to small and finite deformation. In *19<sup>th</sup> UK Conference of the Association for Computational Mechanics in Engineering (ACME), Heriot-Watt University, Edinburgh, UK*, pages 277–280, (2011).
- Ullah, Z., Augarde, C. E., and Coombs, W. M. Adaptive modelling of finite strain shear band localization using the element-free galerkin method. In *20<sup>th</sup> UK Conference of the Association for Computational Mechanics in Engineering (ACME), University of Manchester, Manchester, UK*, pages 251–254, (2012).
- Ullah, Z., Augarde, C. E., and Coombs, W. M. (2013)a, Local maximum entropy shape functions based FE-meshless coupling. Technical Report ECS-TR 2013/07, School of Engineering & Computing Sciences.

- Ullah, Z., Augarde, C. E., and Coombs, W. M. Three-dimensional FE-EFGM adaptive coupling with application to nonlinear adaptive analysis. In *International Conference on Computational Mechanics (CM13), University of Durham, Durham, UK*, (2013)b.
- Ullah, Z., Coombs, W. M., and Augarde, C. E. (2013)c, “An adaptive finite element/meshless coupled method based on local maximum entropy shape functions for linear and nonlinear problems”. *Computer Methods in Applied Mechanics and Engineering*, 267:111–132.
- Vacharasintopchai, T. (2000), A parallel implementation of the element-free Galerkin method on a network of PCs. Master’s thesis, School of Civil Engineering, Asian Institute of Technology, Bangkok, Thailand.
- Valizadeh, N., Bazilevs, Y., Chen, J., and Rabczuk, T. (2015), “A coupled IGA–Meshfree discretization of arbitrary order of accuracy and without global geometry parameterization”. *Computer Methods in Applied Mechanics and Engineering*, 293:20 – 37.
- Walshaw, C. H., Cross, M., and Everett, M. G. (1995), “A Localized Algorithm for Optimizing Unstructured Mesh Partitions”. *International Journal of High Performance Computing Applications*, 9(4):280–295.
- Wang, D. and Zhang, H. (2014), “A consistently coupled isogeometric–meshfree method”. *Computer Methods in Applied Mechanics and Engineering*, 268:843 – 870.
- Wang, H., Li, G., Han, X., and Zhong, Z. H. (2007), “Development of parallel 3D RKPM meshless bulk forming simulation system”. *Advances in Engineering Software*, 38(2):87 – 101.
- Wang, H. P., Wu, C. T., Guo, Y., and Botkin, M. E. (2009), “A coupled meshfree/finite element method for automotive crashworthiness simulations”. *International Journal of Impact Engineering*, 36:1210 – 1222.
- Xiao, Q. and Dhanasekar, M. (2002), “Coupling of FE and EFG using collocation approach”. *Advances in Engineering Software*, 33:507 – 515.
- Yagawa, G., Soneda, N., and Yoshimura, S. (1991), “A Large scale finite element analysis using domain decomposition method on a parallel computer”. *Computers & Structures*, 38:615 – 625.
- Zhuang, X., Augarde, C., and Mathisen, K. (2012)a, “Fracture modeling using meshless methods and level sets in 3D: Framework and modeling”. *International Journal for Numerical Methods in Engineering*, 92(11):969–998.

- Zhuang, X., Heaney, C., and Augarde, C. E. (2012)b, “On error control in the element-free Galerkin method”. *Engineering Analysis with Boundary Elements*, 36(3):351 – 360.
- Zienkiewicz, O. C. and Zhu, J. Z. (1992)a, “The superconvergent patch recovery and a posteriori error estimates. Part 2: Error estimates and adaptivity”. *International Journal for Numerical Methods in Engineering*, 33(7):1365–1382.
- Zienkiewicz, O. C. and Zhu, J. Z. (1992)b, “The superconvergent patch recovery and a posteriori error estimates. Part 1: The recovery technique”. *International Journal for Numerical Methods in Engineering*, 33(7):1331–1364.